Universiteit
Leiden
The Netherlands

Solvent tolerance mechanisms in Pseudomonas putida

Kusumawardhani, H.

Citation

Kusumawardhani, H. (2021, March 11). *Solvent tolerance mechanisms in Pseudomonas putida*. Retrieved from https://hdl.handle.net/1887/3151637

Version:	Publisher's Version
License:	Licence agreement concerning inclusion of doctoral thesis in the Institutional Repository of the University of Leiden
Downloaded from:	https://hdl.handle.net/1887/3151637

Note: To cite this publication please use the final published version (if applicable).

Cover Page

Universiteit Leiden

The handle https://hdl.handle.net/1887/3151637 holds various files of this Leiden University dissertation.

Author: Kusumawardhani, H.
Title: Solvent tolerance mechanisms in Pseudomonas putida
Issue Date: 2021-03-11

CHAPTER 4

A novel toxin-antitoxin module SlvT–SlvA regulates megaplasmid stability and incites solvent tolerance in *Pseudomonas putida* S12

Hadiastri Kusumawardhani, David van Dijk, Rohola Hosseini, Johannes H. de Winde

Published in: Applied and Environmental Microbiology (2020), 86 (13), e00686-20.
DOI: 10.1128/AEM.00686-20

Abstract

Pseudomonas putida S12 is highly tolerant of organic solvents in saturating concentrations, rendering this microorganism suitable for the industrial production of various aromatic compounds. Previous studies revealed that *P. putida* S12 contains a single-copy 583 kbp megaplasmid pTTS12. pTTS12 carries several important operons and gene clusters facilitating *P. putida* S12 survival and growth in the presence of toxic compounds or other environmental stresses. We wished to revisit and further scrutinize the role of pTTS12 in conferring solvent tolerance. To this end, we cured the megaplasmid from *P. putida* S12 and conclusively confirmed that the SrpABC efflux pump is the major determinant of solvent tolerance on the megaplasmid pTTS12. In addition, we identified a novel toxin-antitoxin module (proposed gene names *slvT* and *slvA,* respectively) encoded on pTTS12 which contributes to the solvent tolerance phenotype and is important for conferring stability to the megaplasmid. Chromosomal introduction of the *srp* operon in combination with the *slv*AT gene pair created a solvent tolerance phenotype in non-solvent-tolerant strains such as *P. putida* KT2440, *Escherichia coli* TG1, and *E. coli* BL21(DE3).

Importance

Sustainable alternatives for high-value chemicals can be achieved by using renewable feedstocks in bacterial biocatalysis. However, during bioproduction of such chemicals and biopolymers, aromatic compounds that function as products, substrates or intermediates in the production process may exert toxicity to microbial host cells and limit the production yield. Therefore, solvent tolerance is a highly preferable trait for microbial hosts in the biobased production of aromatic chemicals and biopolymers. In this study, we revisit the essential role of megaplasmid pTTS12 from solvent-tolerant *Pseudomonas putida* S12 for molecular adaptation to an organic solvent. In addition to the solvent extrusion pump (SrpABC), we identified a novel toxin-antitoxin module (SlvAT) which contributes to short-term tolerance in moderate solvent concentrations, as well as to the stability of pTTS12. These two gene clusters were successfully expressed in non-solvent-tolerant strains of *P. putida* and *Escherichia coli* strains to confer and enhance solvent tolerance.

Introduction

One of the main challenges in the production of aromatic compounds is chemical stress caused by the added substrates, pathway intermediates, or products. These chemicals, often exhibiting characteristics of organic solvents, are toxic to microbial hosts and may negatively impact product yields. They adhere to the cell membranes, alter membrane permeability, and cause membrane damage (1, 2). *Pseudomonas putida* S12 exhibits exceptional solvent tolerance characteristics, enabling this strain to withstand toxic organic solvents in saturating concentrations (3, 4). Consequently, a growing list of valuable compounds has successfully been produced using *P. putida* S12 as a biocatalyst by exploiting its solvent tolerance (5–9).

Following the completion of its full genome sequence and subsequent transcriptome and proteome analyses, several genes have been identified that may play important roles in controlling and maintaining solvent tolerance of *P. putida* S12 (10–12). As previously reported, an important solvent tolerance trait of *P. putida* S12 is conferred through the resistance-nodulation-division (RND)-family efflux pump SrpABC, which actively removes organic solvent molecules from the cells (13, 14). Initial attempts to heterologously express the SrpABC efflux pump in *Escherichia coli* enabled the instigation of solvent tolerance and production of 1-naphtol (15, 16). Importantly, the SrpABC efflux pump is encoded on the megaplasmid pTTS12 of *P. putida* S12 (12).

The 583-kbp megaplasmid pTTS12 is a stable single-copy plasmid specific to *P. putida* S12 (12). It harbors several important operons and gene clusters enabling *P. putida* S12 to tolerate, resist and survive the presence of various toxic compounds or otherwise harsh environmental conditions. Several examples include the presence of a complete styrene degradation pathway gene cluster, the RND efflux pump specialized for organic solvents (SrpABC), and several gene clusters conferring heavy metal resistance (12, 17, 18). In addition, through analysis using TADB2.0, a toxin-antitoxin database (19, 20), pTTS12 is predicted to contain three toxin-antitoxin modules. Toxin-antitoxin modules recently have been recognized as important determinants of resistance towards various stress conditions, like nutritional stress and exposure to sublethal concentration of chemical stressor (21, 22). Toxin-antitoxin modules identified in pTTS12 consist of an uncharacterized RPPX_26255-RPPX_26260 system and two identical copies of a VapBC system (23). RPPX_26255 and RPPX_26260 belong to a newly characterized type II toxin-antitoxin pair, COG5654-COG5642. While toxin-antitoxin systems are known to preserve plasmid stability through postsegregational killing of plas-

mid-free daughter cells (24), RPPX_26255-RPPX_26260 was also previously shown to be upregulated during organic solvent exposure, suggesting its role in solvent tolerance (11).

In the manuscript, we further address the role of pTTS12 in conferring solvent tolerance of *P. putida* S12. Curing pTTS12 from its host strain might cause a reduction in solvent tolerance, while complementation of the *srp* operon into the cured strain may fully or partially restore solvent tolerance. Furthermore, we wished to identify additional genes or gene clusters on pTTS12 and putative mechanisms that might also play a role in conferring solvent tolerance to *P. putida* and non-solvent-tolerant *E. coli*.

Results

Megaplasmid pTTS12 is essential for solvent tolerance in *P. putida* S12

To further analyze the role of the megaplasmid of *P. putida* S12 in solvent tolerance, pTTS12 was removed from *P. putida* S12 using mitomycin C. This method was selected due to its reported effectiveness in removing plasmids from *Pseudomonas sp.* (25), although previous attempts regarded plasmids that were significantly smaller in size than pTTS12 (26). After treatment with mitomycin C (10 to 50 mg liter^{-1}), liquid cultures were plated on M9 minimal medium supplemented with indole to select for plasmid-cured colonies. Megaplasmid pTTS12 encodes two key enzymes, namely, styrene monooxygenase (SMO) and styrene oxide isomerase (SOI) that are responsible for the formation of indigo coloration from indole. This conversion results in indigo coloration in spot assays for wild-type *P. putida* S12 whereas white colonies are formed in the absence of megaplasmid pTTS12. With the removal of pTTS12, loss of indigo coloration and, hence, of indigo conversion was observed in all three plasmid-cured strains and the negative control *P. putida* KT2440 (Fig. 4.1A).

With mitomycin C concentration of 30 mg liter^{-1}, 2.4% (3 out of 122) of the obtained colonies appeared to be completely cured from the megaplasmid, underscoring the high genetic stability of the plasmid. No colonies survived the addition of 40 and 50 mg liter^{-1} of mitomycin C, whereas all the colonies that survived the addition of 10 and 20 mg liter^{-1} of mitomycin C retained the megaplasmid. Three independent colonies cured from the megaplasmid were isolated as *P. putida* S12-6, *P. putida* S12-10, and *P. putida* S12-22. The complete loss of the megaplasmid was further confirmed by phenotypic analysis (Fig. 4.1), and by full-genome sequencing. Several operons involved in heavy metal resistance were previously reported

in the pTTS12 (12). The *terZABCD* operon contributes to tellurite resistance in wild-type *P. putida* S12 with minimum inhibitory concentrations (MICs) as high as 200 mg liter^{-1} (Fig. 4.1B). In the megaplasmid-cured strains, a severe reduction of tellurite resistance was observed, decreasing the potassium tellurite MIC to 50 mg liter^{-1} (Fig. 4.1B).

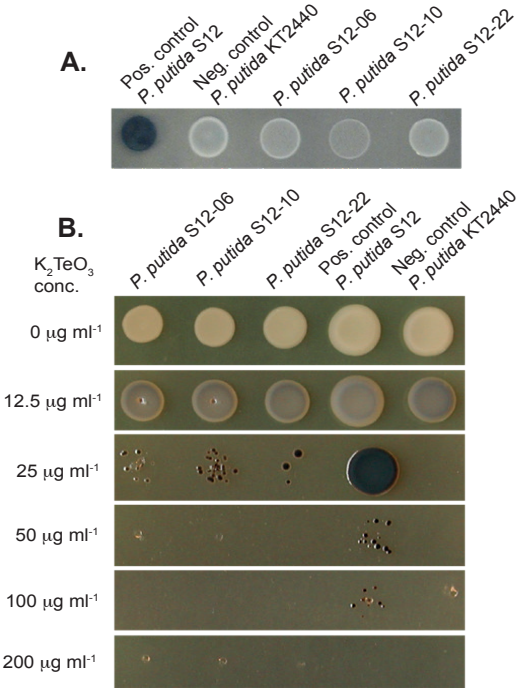

Fig. 4.1. Curing of the megaplasmid pTTS12 from *P. putida* S12.

A. Activity of styrene monooxygenase (SMO) and styrene oxide isomerase (SOI) for indigo formation from indole in *P. putida* strains. Enzyme activity was lost in the megaplasmid-cured genotype S12 ΔpTTS12 (white colonies). Indole (100 mg liter^{-1}) was supplemented in M9 minimum medium.

B. K_2TeO_3 resistance of *P. putida* strains on lysogeny broth (LB) agar. Tellurite resistance was reduced in the megaplasmid-cured genotype S12 ΔpTTS12 (MIC 50 mg liter^{-1}).

Genomic DNA sequencing confirmed a complete loss of pTTS12 from *P. putida* genotypes S12-6, S12-10, and S12-22 without any plasmid-derived fragment being inserted within the chromosome, and genomic alterations by mitomycin C treatment were minimal. Complementation of pTTS12 into the plasmid-cured *P. putida* S12 genotypes restored the indole-indigo transformation and high tellurite resistance to a similar level as the wild-type strain (see Fig. 4.S1 in the supplemental material). Repeated megaplasmid curing experi-

ments indicated that *P. putida* S12 can survive the addition of 30 mg liter^{-1} mitomycin C with the frequency of (2.48 ± 0.58) x 10^{-8}. Among these survivors, only 2% of the colony population lost the megaplasmid, confirming the genetic stability of pTTS12. In addition, attempts to cure the plasmid by introducing double-strand breaks as described by Wynands and colleagues (27) were not successful due to the pTTS12 stability.

Growth comparison in solid and liquid culture in the presence of toluene was performed to analyze the effect of megaplasmid curing in constituting solvent tolerance trait of *P. putida* S12. In contrast with wild-type *P. putida* S12, the plasmid-cured genotypes were unable to grow under toluene atmosphere conditions (data not shown). In liquid LB medium, plasmid-cured *P. putida* S12 genotypes were able to tolerate 0.15% (vol/vol) toluene, whereas the wild-type *P. putida* S12 could grow in the presence of 0.30% (vol/vol) toluene (Fig. 4.2). In the megaplasmid-complemented *P. putida* S12-C genotypes, solvent tolerance was restored to the wildtype level (Fig. 4.S1-D). Hence, the absence of megaplasmid pTTS12 caused a significant reduction of solvent tolerance in *P. putida* S12.

The SrpABC efflux pump and gene pair RPPX_26255-26260 are the main constituents of solvent tolerance encoded on pTTS12

The significant reduction of solvent tolerance in plasmid-cured *P. putida* S12 underscored the important role of megaplasmid pTTS12 in solvent tolerance. Besides encoding the efflux pump SrpABC enabling efficient intermembrane solvent removal (12, 13), pTTS12 carries more than 600 genes and, hence, may contain additional genes involved in solvent tolerance. Two adjacent hypothetical genes, RPPX_26255 and RPPX_26260, were previously reported to be upregulated in a transcriptomic study as a short-term response to toluene addition (11). We propose to name the RPPX_26255-RPPX_26260 gene pair as "*slv"* due to its elevated expression in the presence of solvent. In a first attempt to identify additional potential solvent tolerance regions of pTTS12, we deleted the *srp*ABC genes (Δ*srp*), RPPX_26255-26260 genes (Δ*slv*), and the combination of both gene clusters (Δ*srp* Δ*slv*) from pTTS12 in wild-type *P. putida* S12.

All strains were compared for growth under increasing toluene concentrations in liquid LB medium (Fig. 4.2). In the presence of low concentrations of toluene (0.1% [vol/vol]), all genotypes showed similar growth. With the addition of 0.15% (vol/vol) toluene, S12 Δ*slv*, S12 Δ*srp* and S12 Δ*srp* Δ*slv* exhibited slower growth and reached a lower optical density at 600

nm (OD_{600}) than the wild-type S12 strain. S12 Δ*slv* and S12 Δ*srp* achieved a higher OD_{600} in batch growth than S12 ΔpTTS12 and S12 Δ*srp* Δ*slv* due to the presence of the SrpABC efflux pump or RPPX_26255-RPPX_26260 gene pair.

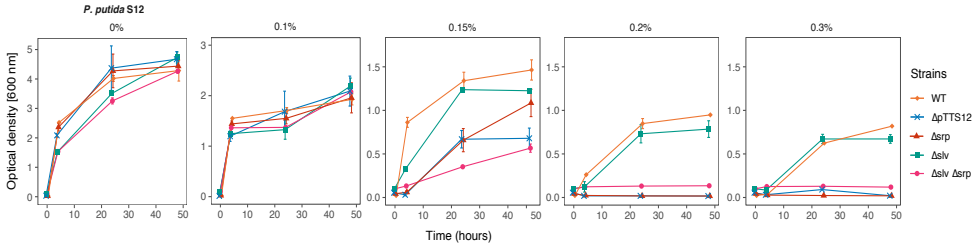

Fig. 4.2. Megaplasmid pTTS12 determines the solvent tolerance trait of *P. putida* S12.

Solvent tolerance analysis was performed on wild-type *P. putida* S12, *P. putida* S12 ΔpTTS12 (genotypes S12-6, S12-10, and S12-22), *P. putida* S12 Δsrp, *P. putida* S12 Δslv, and *P. putida* S12 Δsrp Δslv growing in liquid LB media with 0%, 0.10%, 0.15%, 0.20% and 0.30% (vol/vol) toluene. The removal of the megaplasmid pTTS12 clearly caused a significant reduction in the solvent tolerance of ***P. putida*** S12 ΔpTTS12. Deletion of srpABC (Δsrp), RPPX_26255-26260 (Δslv), and the combination of these gene clusters (Δsrp Δslv) resulted in a lower solvent tolerance. This figure displays the means of three biological replicates, and error bars indicate standard deviation. The range of y axes are different in the first panel (0 to 5), second panel (0 to 3) and third to fifth panels (0 to 1.5).

Interestingly, S12 Δ*srp* Δ*slv* (still containing pTSS12) exhibited diminished growth compared with S12 ΔpTTS12. This may be an indication of megaplasmid burden in the absence of essential genes for solvent tolerance. With 0.2% and 0.3% (vol/vol) toluene added to the medium, S12 Δ*srp,* S12 Δ*srp* Δ*slv*, and S12 ΔpTTS12 were unable to grow, while wild-type S12 and S12 Δ*slv* were able to grow, although S12 Δ*slv* reached a lower OD_{600}. Taken together, these results demonstrate an important role for both the SrpABC efflux pump and the *slv* gene pair in conferring solvent tolerance. We chose *P. putida* S12-6 for further experiments representing megaplasmid-cured *P. putida* S12.

Solvent tolerance can be exerted by ectopic expression of the SrpABC efflux pump and *slv* gene pair in Gram-negative bacteria

The functionality of the *srp* operon and *slv* gene pair was explored in the model Gram-negative non-solvent-tolerant strains *P. putida* KT2440, *E. coli* TG1 and *E. coli* BL21(DE3). We complemented *srpRSABC* (*srp* operon), *slv* gene pair, and a combination of both gene clus-

ters into *P. putida* S12-6, *P. putida* KT2440, *E. coli* TG1, and *E. coli* BL21(DE3) using mini-Tn7 transposition. These strains were chosen due to their common application as model industrial strains while lacking solvent tolerance. *P. putida* KT2440 is another robust microbial host for metabolic engineering due to its adaptation toward physicochemical stresses; however, contrary to P. putida S12, this strain is not solvent-tolerant (28). *E. coli* BL21(DE3), derived from strain B, is the common *E. coli* lab strain optimized for protein production due to its lacking Lon and OmpT proteases and encoding T7 RNA polymerase (29). *E. coli* TG1 was previously reported to successfully produce 1-naphtol with the expression of SrpABC (15, 16), and therefore, this strain was included in this study as a comparison.

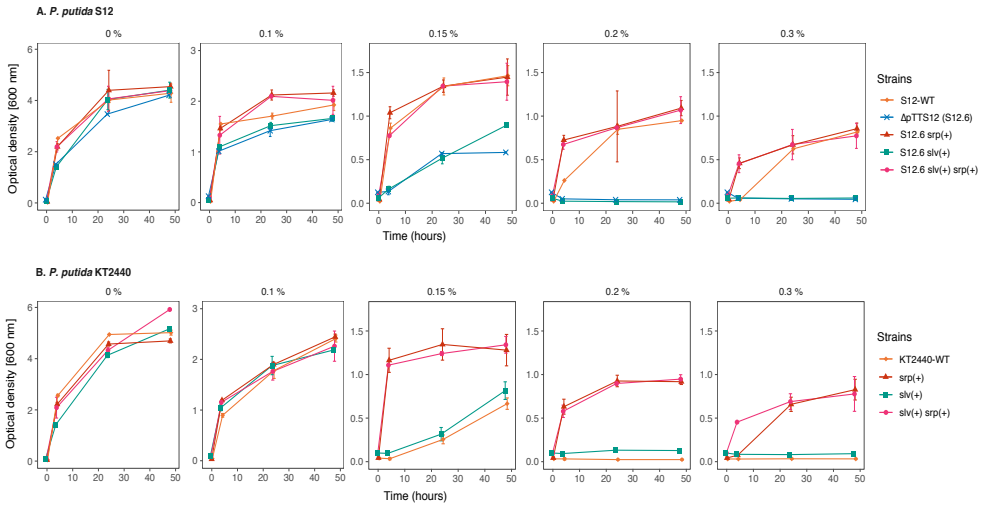

Fig. 4.3. Chromosomal introduction of *srp* and *slv* gene clusters increased solvent tolerance in *P. putida* genotypes.

Solvent tolerance analysis of the genotypes with chromosomal introduction of *srp* operon (*srpRSABC*), *slv* gene pair (RPPX_26255-RPPX_26260), and the combination of these gene clusters into *P. putida* S12 ΔpTTS12 (represented by strain S12-6) (A) and wild-type *P. putida* KT2440 (B) in liquid LB with 0%, 0.10%, 0.15%, 0.20% and 0.30% (vol/vol) of toluene. Wild-type *P. putida* S12 was taken as a solvent-tolerant control strain. This figure displays the mean of three independent replicates, and error bars indicate standard deviation. The range of y axes are different in the first panel (0 to 6), second panel (0 to 3) and third to fifth panels (0 to 1.5).

The chromosomal introduction of *slv* into S12-6 and KT2440 improved growth of the resulting strains at 0.15% (vol/vol) toluene compared with S12-6 and KT2440 (Fig. 4.3). The introduction of *srp* or a combination of *slv* and *srp* enables S12-6 and KT2440 to grow in the

presence of 0.3% (vol/vol) toluene. In KT2440, the introduction of both *slv* and *srp* resulted in a faster growth in the presence of 0.3% (vol/vol) toluene than the addition of only *srp* (Fig. 4.3B). Interestingly, the growth of S12-6 *srp*,*slv* and S12-6 *srp* is better than wild-type S12 (Fig. 4.3A). The observed faster growth of S12-6 *srp*,*slv* and S12-6 *srp* may be due to more efficient growth in the presence of toluene, supported by a chromosomally introduced *srp* operon, than its original megaplasmid localization. Indeed, replication of this large megaplasmid is likely to require additional maintenance energy. To corroborate this, we complemented the megaplasmid lacking the solvent pump (Tc^R::*srpABC*) into *P. putida* S12-6 *srp* resulting in *P. putida* S12-9. Indeed, *P. putida* S12-9 showed further reduced growth in the presence of 0.20 and 0.30 % (vol/vol) toluene (Fig. 4.S2), indicating the metabolic burden of carrying the megaplasmid. We conclude that the SrpABC efflux pump can be regarded as the major contributor to solvent tolerance from pTTS12. The *slv* gene pair appears to promote tolerance of *P. putida* S12 at least under moderate solvent concentrations.

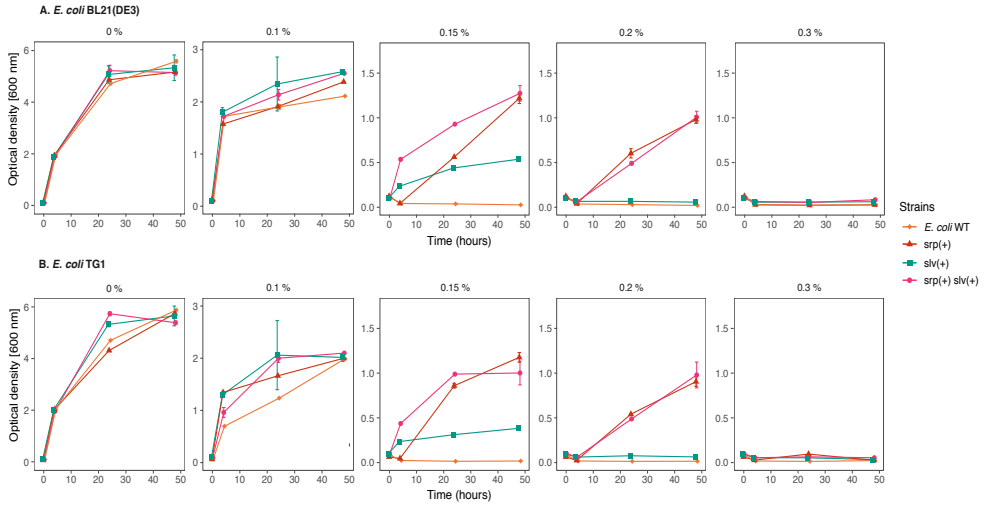

Fig. 4.4. Chromosomal introduction of *srp* and *slv* gene clusters increased solvent tolerance in *E. coli* strains.

Solvent tolerance analysis of the strains with chromosomal introduction of *srp* operon (*srpRSABC*), *slv* gene pair (RPPX_26255-RPPX_26260), and the combination of these gene clusters into *E. coli* BL21(DE3) (A) and *E. coli* TG1 (B) in liquid LB with 0%, 0.10%, 0.15%, 0.20% and 0.30% (vol/vol) of toluene. This figure displays the mean of three independent replicates, and error bars indicate standard deviation. The range of y axes are different in the first panel (0 to 6), second panel (0 to 3) and third to fifth panels (0 to 1.5).

The intrinsic solvent tolerance of *E. coli* strains was observed to be clearly lower than that of *P. putida* (Fig. 4.4). The wild-type *E. coli* strains were able to withstand a maximum 0.10% (vol/vol) toluene, whereas plasmid-cured *P. putida* S12-6 and *P. putida* KT2440 were able to grow in the presence of 0.15% (vol/vol) toluene. With the introduction of *slv* and *srp* in both *E. coli* strains, solvent tolerance was increased up to 0.15% and 0.2% (vol/vol) toluene respectively (Fig. 4.4). A combination of *slv* and *srp* also increased tolerance to 0.20% (vol/vol) toluene, while showing a better growth than the chromosomal introduction of only *srp*. However, none of these strains were able to grow in the presence of 0.30% (vol/vol) toluene.

qPCR analysis of SrpABC expression (Table 4.S1) in *P. putida* S12, *P. putida* KT2440, *E. coli* TG1, and *E. coli* BL21(DE3) confirmed that *srp*A, *srp*B, and *srp*C were expressed at basal levels in all strains. In the presence of 0.10% toluene, the expression of *srp*A, *srp*B, and *srp*C was clearly upregulated in all strains. Thus, the lower solvent tolerance conferred by introducing SrpABC efflux pump in *E. coli* strains was not due to lower expression of the *srp* genes. An analysis of the codon adaptation index (CAI) (http://genomes.urv.es/CAIcal/) (30) showed that for both the *P. putida* and *E. coli* strains, the CAI values of the srp operon are suboptimal, cleary below 0.8 to 1.0 (Table 4.S2). Interestingly, the CAI values were higher for *E. coli* (0.664) than for *P. putida* (0.465), predicting a better protein translation efficiency of the *srp* operon in *E. coli*. Hence, reduced translation efficiency is not likely to be the cause of lower performance of the *srp* operon in *E. coli* strains for generating solvent tolerance. Overall, our results indicate that, in addition to the solvent efflux pump, *P. putida* S12 and *P. putida* KT2440 are intrinsically more robust than *E. coli* TG1 and *E. coli* BL21(DE3) in the presence of toluene.

The *slv* gene pair constitutes a novel toxin-antitoxin system

BLASTp analysis was initiated to further characterize RPPX_26255 and RPPX_26260. This analysis indicated that RPPX_26260 and RPPX_26255 likely represent a novel toxin-antitoxin (TA) system. Through a database search on TADB2.0 (19, 20), we found that RPPX_26260 is a toxin of COG5654 family typically encodes a RES domain-containing protein, which has a conserved arginine (R) – glutamine (E) – serine (S) motif providing a putative active site; and RPPX_26255 is an antitoxin of COG5642 family. Based on its involvement in solvent tolerance, we propose naming the toxin-encoding RPPX_26260 as *slvT* and the antitoxin-encoding RPPX_26255 as *slvA*.

Makarova and colleague identified putative toxin-antitoxin pairs through genome mining of reference sequences in the NCBI database (31). They identified 169 pairs of the COG5654-COG5642 TA system from the reference sequences (Table 4.S3). Here, we constructed a phylogenetic tree of the COG5654-COG5642 TA system, including SlvA (GenBank accession no. AJA16859.1) and SlvT (AJA16860.1), as shown in Fig. 4.5A and 4.6A. SlvA and SlvT cluster with other plasmid-borne toxin-antitoxin from *Burkholderia vietnamensis* G4, *Methylibium petroleiphilum* PM1, *Rhodospirillum rubrum* ATCC 11170, *Xanthobacter autotrophicus* Py2, *Sinorhizobium meliloti* 1021, *Sinorhizobium medicae* WSM419, and *Gloeobacter violaceus* PCC7421. Multiple alignments of SlvAT against the COG5654-COG5642 TA system are shown in Fig. 4.5B and 4.6B.

Of the 169 TA pairs of the COG5654-COG5642 TA system, three TA pairs have recently been characterized, namely, ParST from *Sphingobium sp.* YBL2 (GenBank accession no. AJR25281.1 and AJR25280.1)(32), PP_2433-2434 from *P. putida* KT2440 (NP_744581.1 and NP_744582.1)(33), and MbcAT from *Mycobacterium tuberculosis* H37Rv (NP_216506.1 and NP216505.1)(34), as indicated by bold text and asterisks in Fig. 4.5A and 4.6A. A 3D-model prediction of SlvT and SlvA proteins using the I-TASSER suite for protein structure and function prediction (35), indicated that SlvT and SlvA showed the highest structural similarity to the MbcAT system from *Mycobacterium tuberculosis* (Fig. 4.5C, 4.6C, and 4.S3), which is reported to be expressed during stress conditions (34). Amino acid conservation between SlvAT and these few characterized toxin-antitoxin pairs is relatively low, as they do not belong to the same clade (Fig. 4.5A and 4.6A). However, 100% conservation is clearly observed on the putative active side residues, namely, arginine (R) 35, tyrosine (Y) 45, and glutamine (E) 56, and only 75% consensus is shown on serine (S) 133 residue (Fig. 4.S3).

According to the model with highest TM score, SlvT is predicted to consist of four beta sheets and four alpha helices. As such, SlvT shows structural similarity with diphtheria toxin which functions as an ADP-ribosyl transferase enzyme. Diphtheria toxin can degrade NAD^+ into nicotinamide and ADP ribose (36). A similar function was recently identified for COG5654 family toxins from *P. putida* KT2440, *M. tuberculosis*, and *Sphingobium sp* (32–34).

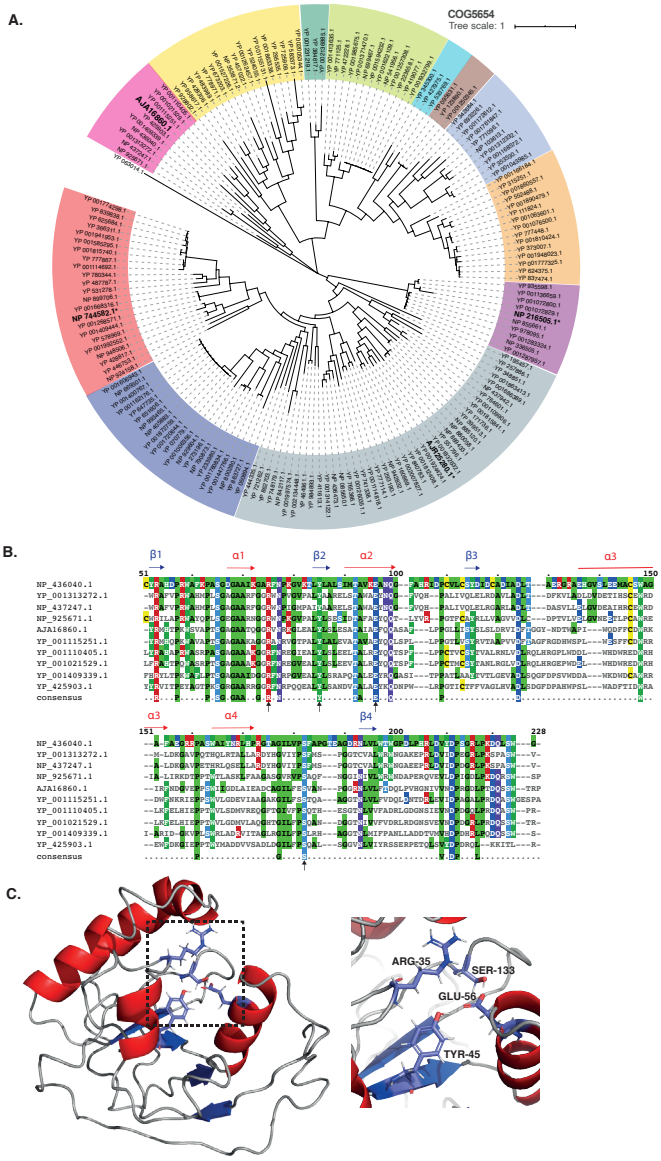

Fig. 4.5. Bioinformatics analysis of SlvT as a member of COG5654 toxin family

A. Phylogenetic tree (neighbour joining tree with 100 bootstraps) of COG5654 family toxin from reference sequences identified by Makarova and colleagues (31). Different colours correspond to the different toxin-antitoxin module clades. Asterisks (*) and bold text indicate the characterized toxin proteins, namely, ParT from *Sphingobium sp.* YBL2 (GenBank accession no. AJR25280.1), PP_2434 from *P. putida* KT2440 (NP_744582.1), MbcT from *Mycobacterium tuberculosis* H37Rv (NP_216505.1), and SlvT from *P. putida* S12 (AJA16860.1).

B. Multiple sequence alignment of the COG5654 toxin SlvT from *P. putida* S12 with several putative COG5654 family toxin proteins which belong in the same clade. Putative active site residues are indicated by black arrows.

C. Protein structure modelling of SlvT using I-TASSER server (35), which exhibits high structural similarity with MbcT from *Mycobacterium tuberculosis* H37Rv. Shown are the close ups of putative active sites of the SlvT toxin (Arg-35, Tyr-45, Glu-56, and Ser-133).

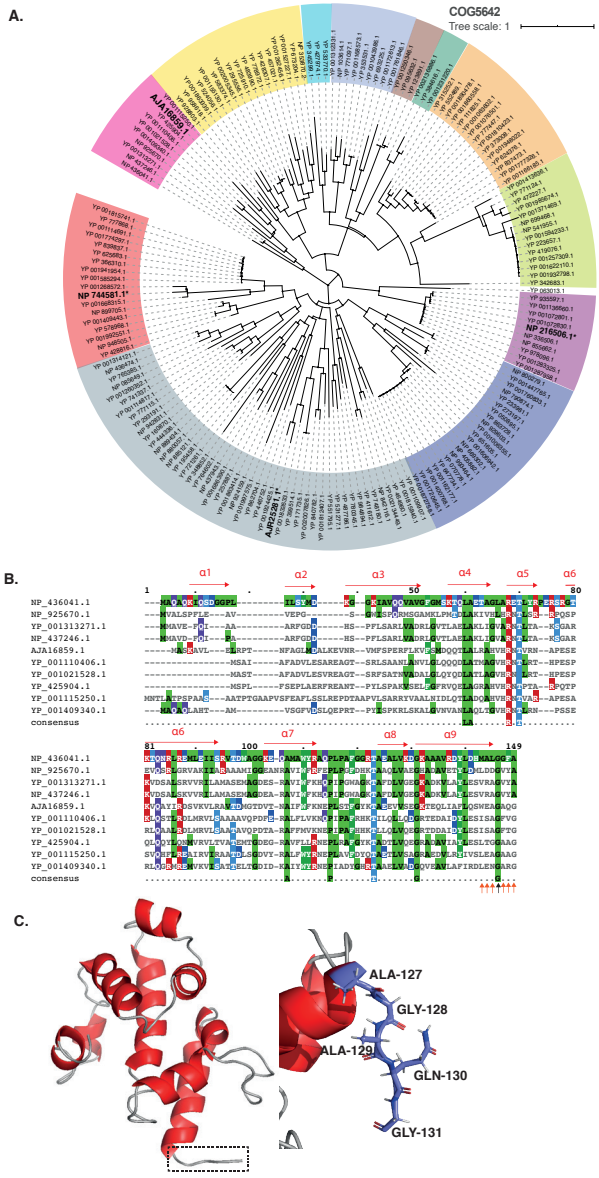

Fig. 4.6. Bioinformatics analysis of SlvA as a member of COG5642 toxin family

A. Phylogenetic tree (neighbour joining tree with 100 bootstrap) of COG5642 family antitoxin from reference sequences identified by Makarova and colleagues (31). Different colours correspond to the different toxin-antitoxin module clades. Asterisks (*) and bold text indicate the characterized antitoxin proteins, namely, ParS from

Sphingobium sp. YBL2 (GenBank accession no. AJR25281.1), PP_2433 from *P. putida* KT2440 (NP_744581.1), MbcA from *Mycobacterium tuberculosis* H37Rv (NP_216506.1), and SlvA from *P. putida* S12 (AJA16859.1).

B. Multiple sequence alignment of the COG5654 toxin SlvA from *P. putida* S12 with several putative COG5642 family antitoxin proteins which belong in the same clade. Putative active site residues are indicated by orange and black arrows.

C. Protein structure modelling of SlvA using I-TASSER server (30) which exhibits high structural similarity with MbcA from *Mycobacterium tuberculosis* H37Rv. Shown are the close up of antitoxin putative C-terminal binding site to block SlvT toxin active site (Ala-127, Gly-128, Ala-129, Gln-130, and Gly-131).

slvT toxin causes cell growth arrest by depleting cellular NAD^+

To prove that *slvAT* presents a pair of toxin and antitoxin, *slvA* and *slvT* were cloned separately in pUK21 (lac-inducible promoter) and pBAD18 (ara-inducible promoter), respectively. The two constructs were cloned into *E. coli* BL21(DE3). The growth of the resulting strains was monitored during conditional expression of the *slvA* and *slvT* genes (Fig. 4.7A). At the mid-log growth phase, a final concentration of 0.8% arabinose was added to the culture (*), inducing expression of *slvT*. After 2 h of induction, growth of this strain ceased, while the uninduced control culture continued to grow. Upon addition of 2 mM isopropyl-β-D-thiogalactopyranoside (IPTG) (**), growth of the *slvT*-induced culture was immediately restored, reaching a similar OD_{600} as the uninduced culture.

Bacterial cell division was further studied by flow cytometer analyses during the expression of *slvT* and *slvA*. After approximately 6 h of growth (indicated by grey arrow in Fig. 4.7A), samples were taken from control, arabinose, and arabinose + IPTG-induced liquid culture. Cell morphology was analyzed by light microscopy, and the DNA content of the individual cells in the culture was measured using a flow cytometer with SYBR green II staining (Fig. 4.7B). Indeed, an absence of dividing cells and lower DNA content were observed during the induction of only *slvT* toxin with arabinose (Fig. 4.7B). Subsequent addition of IPTG to induce *slvA* expression was shown to restore cell division and to an upshift of DNA content similar to that of control strain (Fig. 4.7B). While the expression of *slvT* was not observed to be lethal to bacterial strain, this experiment showed that the expression of the *slvT* toxin stalled DNA replication and, subsequently, cell division. The induction of *slvA* subsequently restored bacterial DNA replication and cell division.

To corroborate a putative target of SlvT, concentrations of NAD^+ were measured during the induction experiment (Fig. 4.7C). Before the addition of arabinose to induce *slvT*

(orange arrow on Fig. 4.7A), NAD^+ was measured and compared to the strain harboring empty pUK21 and pBAD18 (Fig. 4.7B). On average, at this time point, the NAD^+ level is similar between the *slvAT*-bearing strain and the control strain. NAD^+ was measured again after arabinose induction when the growth of the induced strain has diminished (blue arrow on Fig. 4.7A). At this time point, the measured NAD^+ was 32% (±14.47) of the control strain. After the induction of *slvA*, NAD^+ was immediately restored to a level of 77% (±9.97) compared to the control strain. Thus, the induction of *slvT* caused a depletion of NAD^+, while induction of *slvA* immediately increased NAD^+ level, indicating that *slvAT* is a pair of toxin-antitoxin which controls its toxicity through NAD^+ depletion.

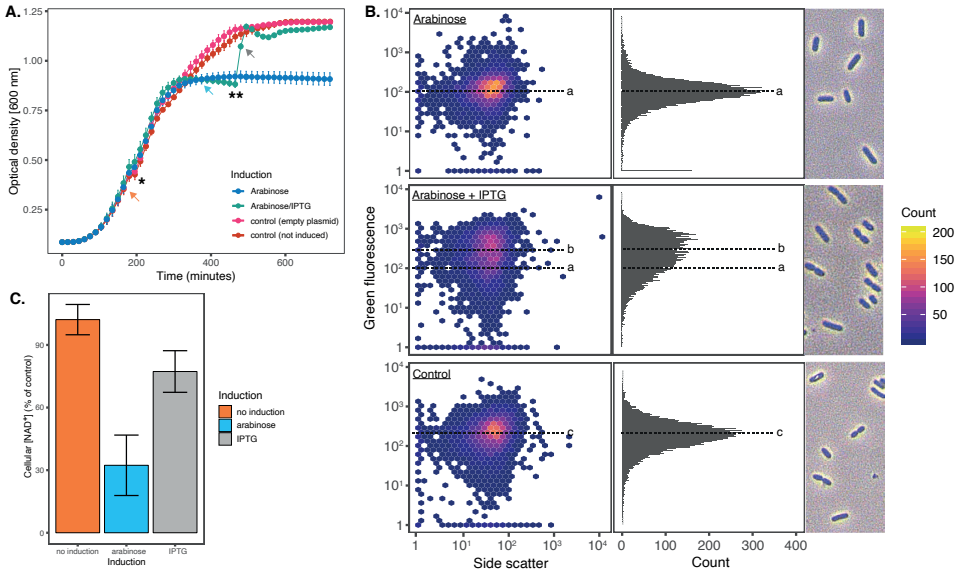

Fig. 4.7. Heterologous expression of SlvAT in *E. coli* BL21(DE3)

A. Growth curves of *E. coli* BL21(DE3) harbouring pBAD18-slvT and pUK21-slvA, showing growth reduction after the induction of toxin by a total concentration of 0.8 % arabinose (*) and growth restoration after antitoxin induction by a total concentration of 2 mM IPTG (**). Samples were taken at the time points indicated by coloured arrows for cellular NAD^+ measurement.

B. Flow cytometry analysis of DNA content and cell morphology visualization on *E. coli* BL21(DE3) during *slvT* and *slvAT* expression. Median value of green fluorescence representing DNA content during *slvT* expression (118.202), *slvAT* expression (236.056), and control (208.406) are indicated by **a**, **b**, and **c**, respectively. Samples were taken at the time point indicated by grey arrow in A.

C. Cellular NAD^+ measurements during the expression of the toxin-antitoxin module. Induction of toxin SlvT caused a reduction in cellular NAD^+ level to 32.32% (±14.47%) of the control strain, while the expression of SlvA

restored cellular NAD^+ level to 77.27% (±9.97%) of the control strain.

slvAT regulates megaplasmid pTTS12 stability

In addition to its role in solvent tolerance, localization of the *slvAT* pair on megaplasmid pTTS12 may have an implications for plasmid stability. pTTS12 is a very stable megaplasmid that cannot be spontaneously cured from *P. putida* S12 and cannot be removed by introducing double-strand breaks (see above). We deleted *slvT* and *slvAT* from the megaplasmid to study their impact in pTTS12 stability. With the deletion of *slvT* and *slvAT*, the survival rate during treatment with mitomycin C improved significantly, reaching (1.01 ± 0.17) x 10^{-4} and (1.25 ± 0.81) x 10^{-4}, respectively, while the wild-type S12 had a survival rate of (2.48 ± 0.58) x 10^{-8}.

We determined the curing rate of pTTS12 from the surviving colonies. In wild-type S12, the curing rate was 2% (see also above), while in Δ*slvT* and Δ*slvAT* mutants, the curing rate increased to 41.3% (± 4.1%) and 79.3% (± 10%), respectively, underscoring an important role for *slvAT* in megaplasmid stability. We attempted to cure the megaplasmid from the colonies by introducing a double strand break (DSB), as previously described on *Pseudomonas taiwanensis* VLB120 (27, 37). This indeed was not possible in wild-type S12 and Δ*slvT* strains; however, the Δ*slvAT* mutant now showed plasmid curing by a DSB, resulting in a curing rate of 34.3% (± 16.4%).

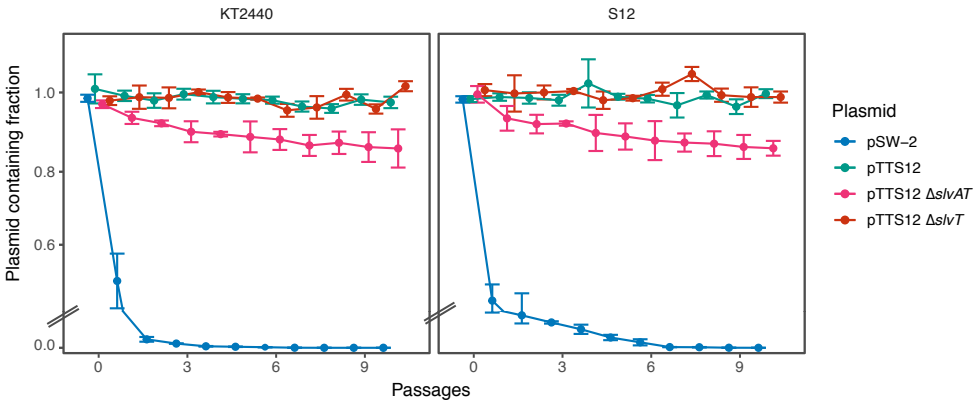

Fig. 4.8. SlvAT is important for pTTS12 maintenance in *P. putida*.

pTTS12 (variant with Km^R) maintenance in *P. putida* S12 and *P. putida* KT2440 growing in LB liquid medium without antibiotic selection for 10 passages (approximately 10 generations per passage). pSW-2 was taken as negative control for plasmid stability in *P. putida*. This experiment was performed with three biological replicates,

and error bars represent standard deviation.

Since Δ*slvT* and Δ*slvAT* may compromise megaplasmid stability, we now performed megaplasmid stability tests by growing S12 and KT2440 harboring pSW-2 (negative control) (37), pTTS12 (positive control), pTTS12 Δ*slvT*, and pTTS12 Δ*slvAT* in LB medium with 10 passages (± 10 generations/passage step) as shown in Fig. 4.8. Both KT2440 and S12 easily lost the negative-control plasmid pSW-2 (Fig. 4.8). Plasmid pTTS12 was not lost during this test, confirming that pTTS12 is indeed a stable plasmid. Furthermore, the Δ*slvT* genotypes also did not show a loss of the megaplasmid. Interestingly, the Δ*slvAT* genotypes spontaneously lost the megaplasmid, confirming that the *slvAT* module is not only important to promote solvent tolerance but also determines megaplasmid stability in *P. putida* S12 and KT2440.

Discussion

Revisiting the role of pTTS12 and SrpABC efflux pump in solvent tolerance

In this study, we conclusively confirm the role of SrpABC efflux pump carried on pTTS12 and identify a novel toxin-antitoxin module playing an additional role in conveying solvent tolerance to P. putida S12 (Fig. 4.9). Notably, megaplasmids may cause a metabolic burden to their host strains, and they can be a source of genetic instability (11). Our results show that, indeed, pTTS12 imposed a metabolic burden in the presence of an organic solvent (Fig. 4.S2). This plasmid is very large and contains many genes that are not related to solvent tolerance. Hence, it may be interesting for biotechnological purposes to reduce plasmid size and, consequently, metabolic burden. In addition, a streamlined and minimal genome size is desirable for reducing host interference and genome complexity (12, 13).

We investigated the heterologous expression of the SrpABC efflux pump in strains of both *P. putida* and *E. coli*, which successfully enhanced their solvent tolerance in these strains (Fig. 4.3 and 4.4). Previous reports on the implementation of SrpABC in whole-cell biocatalysis successfully increased the production of 1-naphtol in *E. coli* TG1 (15, 16). Production was still higher using *P. putida* S12, as this strain could better cope with substrate (naphthalene) toxicity, while both *P. putida* S12 and *E. coli* TG1 showed similar tolerance to the product 1-naphtol (16). In our experiments, the *E. coli* strains clearly showed a smaller increase in toluene tolerance than the *P. putida* strains, although *srpABC* was expressed at a basal level and upregulated in the presence of 0.10 % (vol/vol). These results indicate that besides hav-

ing an efficient solvent efflux pump, *P. putida* S12 and *P. putida* KT2440 are inherently more robust in the presence of toluene and, presumably, other organic solvents than *E. coli* TG1 and *E. coli* BL21(DE3). The absence of cis-trans isomerase (*cti*), resulting in the inability to switch from *cis*- to *trans*-fatty acid in *E. coli* (38), may contribute to this difference in solvent tolerance. Additionally, *P. putida* typically has a high NAD(P)H regeneration capacity (39, 40) which can contribute to the maintenance of proton motive force during solvent extrusion by RND efflux pump. Further detailed investigation is required to reveal the exact basis for its intrinsic robustness.

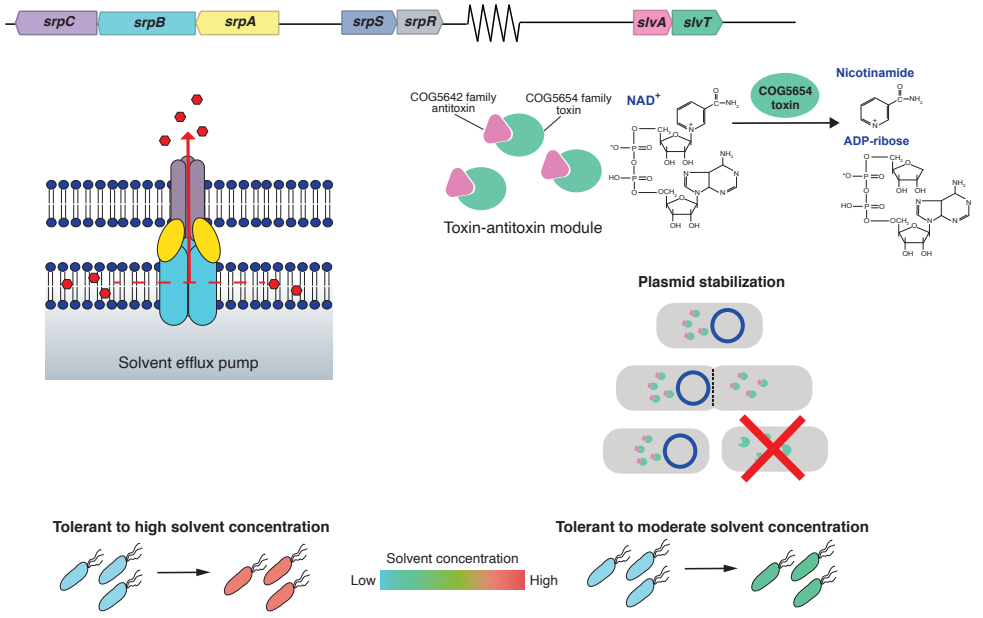

Fig. 4.9. Schematic representation of the gene clusters involved in solvent tolerance from megaplasmid pTTS12.

The SrpABC efflux pump is the major contributor of solvent tolerance trait from the megaplasmid pTTS12. This efflux pump is able to efficiently extrude solvents from membrane lipid bilayer. A COG5654-COG5642 family toxin-antitoxin module (SlvT and SlvA, respectively) promoted the growth of *P. putida* S12 in the presence of a moderate solvent concentration and stabilized pTTS12 plasmid. In the absence of SlvA, SlvT causes toxicity by conferring cellular NAD^+ depletion and, subsequently, halt DNA replication and cell division.

Identification of the novel antitoxin-toxin module SlvAT

In *P. putida* S12, deletion of *srpABC* genes still resulted in higher solvent tolerance than the pTTS12-cured genotypes (Fig. 4.2, panel 3). This finding indicated that within pTTS12 there were other gene(s) which may play a role in solvent tolerance. Two genes of unknown

function were upregulated in a transcriptome analysis of toluene-shocked *P. putida*, namely, RPPX_26255 and RPPX_26260, suggesting a putative role in solvent tolerance (11). Here, we confirmed this finding and demonstrated that these genes together form a novel toxin-antitoxin module (Fig. 4.7). SlvT exerts toxicity by degradation of NAD^+, like other toxins of the COG5654-family, and expression of antitoxin SlvA immediately restored NAD^+ levels. Depletion of NAD^+ interfered with DNA replication and caused an arrest of cell division similar to another recently described COG5654-COG5642 family toxin-antitoxin pair (33). Indeed, the SlvAT toxin-antitoxin module was shown to be important for the stability of pTTS12 (Fig. 4.8).

Based on TADB2.0 analysis, pTTS12 encodes three TA pairs, namely, SlvAT and two identical copies of VapBC. VapBC was first identified from a virulence plasmid of *Salmonella sp.* and is known to prevent the loss of plasmid during nutrient-limiting condition (39). A previous report showed that VapBC can stabilize/retain approximately 90% of pUC plasmid in *E. coli* within 300 h of growth (40), which is similar to our result although demonstrated in a much smaller plasmid and under the control of the lac operon. Serendipitous plasmid loss due to double-strand break was reported in pSTY, which carries two identical copies of VapBC (27). Here, we observed a similar phenomenon in pTTS12 Δ*slvAT*. Hence, in the absence of SlvAT, two copies of VapBC were not sufficient to prevent the loss of pTTS12 on rich media without selection pressure and by double-strand break, indicating a major role for SlvAT.

A putative role of toxin-antitoxin module SlvAT in solvent tolerance

Toxin-antitoxin modules are known to be important in antibiotic persistent strains as a trigger to enter and exit the dormant state, causing the cell to become unaffected by the antibiotic (21, 40, 41). Among *Pseudomonas* species, several toxin-antitoxin modules are reported to be involved in survival strategies, such as stress response, biofilm formation, and antimicrobial persistence (33, 41, 42). Previous transcriptomic studies reported upregulation of the *slvAT* locus as a response towards toluene addition and its expression at 10 to 30 minutes after toluene addition (11). Here, we show that SlvAT improves solvent tolerance in *P. putida* and *E. coli* strains independent of pTTS12 or SrpABC efflux pump. We hypothesize that SlvAT plays a role as a rapid response towards toluene addition. Activation of SlvT toxin may halt bacterial growth, and this allows physiological adaptation and adjustments to take place (e.g., expression of extrusion pumps and membrane compaction) before resuming its growth and cell division in the presence of toxic organic solvent. It is interesting to note that *P. putida* S12

and KT2440 both carry another COG5654-COG5642 family toxin-antitoxin pair in their chromosome (locus tag RPPX_19375-RPPX_19380 and PP_2433-PP_2434, respectively). In *P. putida* S12, this TA module is not being induced during solvent stress, rendering it unlikely to play a role in solvent tolerance.

The putative regulation mechanism of toxin-antitoxin module SlvAT in *P. putida S12*

Expression of the *slvAT* locus with its native promoter region seemed to exert a similar physiological effect in solvent tolerance both in *E. coli* and *P. putida* (Fig. 4.3 and Fig. 4.4). Typically, toxin-antitoxin can regulate its own expression by antitoxin binding to the promoter region (21). Unstable antitoxin is encoded upstream of the stable toxin, giving a transcriptional advantage for production of antitoxin (43). While this study presents the role of SlvAT module as a response to solvent stress, this toxin-antitoxin module may play a role in the response to various other stresses since pTTS12 itself encodes several modules involved in different stress response. It would be interesting to further study whether organic solvents directly induce the expression of *slvAT* locus or intermediate signalling pathways are required. Several type II toxin-antitoxin modules are known to be regulated by proteases, such as Lon and Clp (44). These proteases degrade antitoxin protein, promoting toxin activity, and thus upregulate the expression of the toxin-antitoxin locus. Indeed, our preliminary transcriptomic data show upregulation of specific protease-encoding loci after toluene addition. These may constitute putative regulatory proteases to the SlvAT module. Future research on the dynamics of *slvAT* locus regulation is required for revealing the details of the control mechanisms operating in vivo.

Conclusions

In summary, our experiments confirmed that the SrpABC efflux pump is the major contributor of solvent tolerance on the megaplasmid pTTS12 which can be transferred to other non-solvent-tolerant host microbes. In addition, the megaplasmid carries the novel toxin-antitoxin system SlvAT (RPPX_26255 and RPPX_26260) which promotes rapid solvent tolerance in *P. putida* S12 and is important for maintaining the plasmid stability of pTTS12. Chromosomal introduction of the *srpRSABC* operon genes in combination with *slvAT* confers a clear solvent tolerance phenotype in other industrial strains previously lacking this phenotype, such as *P. putida* KT2440, *E. coli* TG1, and *E. coli* BL21(DE3). Taken together, our findings shows that

both SrpABC and SlvAT constitute suitable candidate loci for exchange with various microbial hosts for increasing tolerance towards toxic compounds.

Materials and Methods

Strains and culture conditions

Strains and plasmids used in this paper are listed in Table 4.1. All *P. putida* strains were grown in Lysogeny Broth (LB) at 30 °C with 200 rpm shaking. *E. coli* strains were cultivated in LB at 37 °C with 250 rpm shaking. For solid cultivation, 1.5 % (wt/vol) agar was added to LB. M9 minimal medium was supplemented with 2 mg liter^{-1} $MgSO_4$ and 0.2 % of citrate as sole carbon source (45). Toluene atmosphere growth was evaluated on solid LB in a glass plate incubated in an exicator with toluene supplied through the gas phase at 30 °C. Solvent tolerance analysis was performed by growing *P. putida* S12 genotypes in LB starting from OD_{600} of 0.1 in Boston bottles with Mininert bottle caps. When required, gentamicin (25 mg liter^{-1}), ampicillin (100 mg L^{-1}), kanamycin (50 mg liter^{-1}), indole (100 g liter^{-1}), potassium tellurite (6.75 to 200 mg liter^{-1}), arabinose (0.8% wt/vol), and IPTG (2 mM) were added to the medium.

Table 4.1. Strains and plasmids used in this paper

Strain	Characteristics	Ref.
P. putida S12	Wild-type *P. putida* S12 (ATCC 700801), harboring megaplasmid pTTS12	(3)
P. putida S12-1	*P. putida* S12, harboring megaplasmid pTTS12 with Km^R marker	This paper
P. putida S12-6/ S12-10/ S12-22	ΔpTTS12	This paper
P. putida S12-9	ΔpTTS12, Gm^R *srpRSABC*::Tn7, complemented with megaplasmid pTTS12 (Tc^R::*srpABC*)	This paper
P. putida S12-C	*P. putida* ΔpTTS12 (S12-6/ S12-10/ S12-22), complemented with megaplasmid pTTS12	This paper
P. putida KT2440	Derived from wild-type *P. putida* mt-2, ΔpWW0	(48)
E. coli HB101	*recA pro leu hsdR* Sm^R	(49)
E. coli BL21(DE3)	*E. coli* B, F^- *ompT gal dcm lon hsdS*$_B$($r_B^-m_B^-$) λ(DE3) [*lacI lacUV5-T7p07 ind1 sam7 nin5*]) [*malB*$^+$]$_{K\text{-}12}$(λ^S)	(29)
E. coli DH5α λpir	*sup* E44, Δ*lacU*169 (Φ*lacZ*ΔM15), *recA*1, *endA*1, *hsdR*17, *thi*-1, *gyrA*96, *relA*1, λpir phage lysogen	(50)
E. coli TG1	*E. coli* K-12, *glnV44 thi-1* Δ*(lac-proAB)* Δ*(mcrB-hsdSM)5*($r_K^-m_K^-$) F′ [*traD36 proAB*$^+$ *lacI*^{q} *lacZΔM15*]	Lucigen
E. coli WM3064	*thrB1004 pro thi rpsL hsdS lacZ*ΔM15 RP4-1360 Δ(*araBAD*)567 Δ*dapA1341*::[erm pir]	William Metcalf

Plasmid		
pRK2013	RK2-Tra$^+$, RK2-Mob$^+$, Km^R, *ori* ColE1	(51)
pEMG	Km^R, Ap^R, *ori* R6K, *lacZ*α MCS flanked by two I-SceI sites	(37)
pEMG-Δ*srpABC*	pEMG plasmid for constructing *P. putida* S12 Δ*srpABC*	This paper
pEMG-Δ*slvAT*	pEMG plasmid for constructing *P. putida* S12 Δ*slvAT*	This paper
pEMG-Δ*slvT*	pEMG plasmid for constructing *P. putida* S12 Δ*slvT*	This paper
pSW-2	Gm^R, *ori* RK2, *xylS*, Pm ® I-sceI	(37)
pBG35	Km^R, Gm^R, *ori* R6K, pBG-derived	(46)
pBG-srp	Km^R, Gm^R, *ori* R6K, pBG-derived, contains *srp* operon (RPPX_27995-27965)	This paper
pBG-slv	Km^R, Gm^R, *ori* R6K, pBG-derived, contains *slv* gene pair (RPPX_26255-26260)	This paper
pBG-srp-slv	Km^R, Gm^R, *ori* R6K, pBG-derived, contains *slv* gene pair (RPPX_26255-26260) and *srp* operon (RPPX_27995-27965)	This paper
pBAD18-slvT	Ap^R, ara operon, contains *slvT* (RPPX_26260)	This paper
pUK21-slvA	Km^R, lac operon, contains *slvA* (RPPX_26255)	This paper
pTnS-1	Ap^R, *ori* R6K, TnSABC+D operon	(52)

DNA and RNA methods

All PCRs were performed using Phusion polymerase (Thermo Fisher) according to the manufacturer's manual. Primers used in this paper (Table 4.2) were procured from Sigma-Aldrich. PCR products were checked by gel electrophoresis on 1 % (wt/vol) TBE agarose containing 5 µg ml^{-1} ethidium bromide (110V, 0.5x TBE running buffer). For reverse transcriptase quantitative PCR (RT-qPCR) analysis, RNA was extracted using TRIzol reagent (Invitrogen) according to the manufacturer's manual. The obtained RNA samples were immediately reverse transcribed using iScript cDNA synthesis kit (Bio-Rad), and cDNA may have been stored at -20 °C prior to qPCR analysis. qPCR was performed using iTaq Universal SYBR Green Supermix (Bio-Rad) on a CFX96 Touch real-time PCR Detection System (Bio-Rad). The genome sequence of *P. putida* S12 ΔpTTS12 was analyzed using Illumina HiSeq instrument (GenomeScan BV, The Netherlands) and assembled according to the existing complete genome sequence (GenBank accession no. CP009974 and CP009975) (12).

Table 4.2. Oligos used in this study

Oligos	Sequences (5'-3')	Restriction sites	PCR templates	Description
TS1-srp-for	TATCTGGTACCTTGTCCTGGAAG CCGCTAATGA	KpnI	pTTS12	Construction of pEMG-Δ*srpABC*
TS1-srp-rev	CAGCGGCGGCCGCTTTAACGCA GGAAAGCTGCGAG	NotI	pTTS12	Construction of pEMG-Δ*srpABC*
TS2-srp-for	CCGAAGCGGCCGCCAGCGCAG TTAAGGGGATTACC	NotI	pTTS12	Construction of pEMG-Δ*srpABC*
TS2-srp-rev	TCAGCTCTAGAGCGCAGGTAAG GCTTCACC	XbaI	pTTS12	Construction of pEMG-Δ*srpABC*
srpO_F	TGCGAATTCGGTATCGCACATG GCATTGG	EcoRI	pTTS12	Construction of pBG-srp
srpO_R	TGCTCTAGAGCCTCACACCTGG TGTACC	XbaI	pTTS12	Construction of pBG-srp
slv_F	ATGCTTAATTAACTTTTGCTGCG GTCTACACAGG	PacI	pTTS12	Construction of pBG-slv
slv_R	AGCGGGAATTCCTCCAAAACCG GTTCTGAAGCC	EcoRI	pTTS12	Construction of pBG-slv
slvA_F	AGAGAGCTCCATAGTAAGTGCA ATCCTAAAG	SacI	pTTS12	Construction of pUK21-*slvA*
slvA_R	GTCTAGACTCCAGCTCCAGATG TAG	XbaI	pTTS12	Construction of pUK21-*slvA*
slvT_F	GGTGCTCTAGAATGAAAATCATC GGAGTG	XbaI	pTTS12	Construction of pBAD18-*slvT*
slvT_R	GGAAGGAGCTCGTACGTGTAAG GCGCTAC	SacI	pTTS12	Construction of pBAD18-*slvT*
TS1_slv_F	TGCTGGAATTCCTTTTGCTGCGG TCTACACAGG	EcoRI	pTTS12	Construction of pEMG-Δ*slvAT*
TS1_slv_R	GGCAACTGATCGGTGAAAAGCAC TTTGAGAGCGTCCATCAAGCC	-	pTTS12	Construction of pEMG-Δ*slvAT*
TS2_slv_F	GGCTTGATGGACGCTCTCAAAGT GCTTTTCACCGATCAGTTGC	-	pTTS12	Construction of pEMG-Δ*slvAT*
TS2_slv_R	GCCCAGGATCCCGAATGTCCATA ATCCAGGCGC	KpnI	pTTS12	Construction of pEMG-Δ*slvAT*
TS1_slvT_F	GCATAGGATCCGAGAATTGTGCAT AGTAAGTG	KpnI	pTTS12	Construction of pEMG-Δ*slvT*
TS1_slvT_R	GATCGTTGACCACAATATCTCCAG CTCCAGATGTAG	-	pTTS12	Construction of pEMG-Δ*slvT*
TS2_slvT_F	CTACATCTGGAGCTGGAGATATTG TGGTCAACGATC	-	pTTS12	Construction of pEMG-Δ*slvT*
TS2_slvT_R	AGGTTAAGCTTGTCTGCAGTGTCT ATTCC	HindIII	pTTS12	Construction of pEMG-Δ*slvT*
eco_gyrB_F	CGATAATTTTGCCAACCAC-GAT	-	gyrB	qPCR, reference gene
eco_gyrB_R	GAAATTCTCCTCCCAGAC-CAAA	-	gyrB	qPCR, reference gene

Oligos	Sequences (5'-3')	Restriction sites	PCR templates	Description
eco_rpoB_F	AACACGAGTTC-GAGAAGAAACT	-	rpoB	qPCR, reference gene
eco_rpoB_R	CGTTTAACCGCCAGA-TATACCT	-	rpoB	qPCR, reference gene
ppu_gyrB_F	GCTTCGACAAGATGATTTC-GTC	-	gyrB	qPCR, reference gene
ppu_gyrB_R	GCAGTTTGTCGATGTTG-TACTC	-	gyrB	qPCR, reference gene
ppu_rpoB_F	GACAAGGAATCGTCGAA-CAAAG	-	rpoB	qPCR, reference gene
ppu_rpoB_R	GAAGGTACCGTTCTCAGT-CATC	-	rpoB	qPCR, reference gene
srpA_F	CTCGGAAAACTTCA-GAGTTCCT	-	srpA	qPCR, target gene
srpA_R	AAAGCTTCTTGGTCTG-CAAAAG	-	srpA	qPCR, target gene
srpB_F	TACATGACCAGGAAGACCAG-TA	-	srpB	qPCR, target gene
srpB_R	GTGGAGGTCATTTATC-CCTACG	-	srpB	qPCR, target gene
srpC_F	GCCATAAGTTGATGTTCAG-CAG	-	srpC	qPCR, target gene
srpC_R	ATTCCAACGGATTTGC-CAAAAA	-	srpC	qPCR, target gene

Curing and complementation of megaplasmid pTTS12 from *P. putida* S12

P. putida S12 was grown in LB to reach early exponential phase (approximately 3 h or OD_{600} 0.4-0.6). Subsequently, mitomycin C was added to the liquid LB culture to a final concentration of 10, 20, 30, 40, or 50 μg ml^{-1}. These cultures were grown for 24 h and plated on M9 minimal media supplemented with indole to select for the absence of megaplasmid. Loss of megaplasmid was confirmed by loss of other phenotypes connected with the megaplasmid, such as MIC reduction of potassium tellurite and solvent sensitivity under toluene atmosphere, as well as through genomic DNA sequencing. Complementation of megaplasmid pTTS12 was performed using biparental mating between *P. putida* S12-1 (pTTS12 Km^R) and plasmid-cured genotypes *P. putida* S12 ΔpTTS12 (Gm^R :: Tn7) and followed by selection on LB agar supplemented with kanamycin and gentamicin.

Plasmid cloning

Deletion of *srpABC*, *slvT*, and *slvAT* genes was performed using homologous recombination between free-ended DNA sequences that are generated by cleavage at unique I-SceI sites

(37). Two homologous recombination sites were chosen downstream (TS-1) and upstream (TS-2) of the target genes. TS-1 and TS-2 fragments were obtained by performing PCR using primers listed in Table 4.2. Constructs were verified by DNA sequencing. Mating was performed as described by Wynands and colleagues (27). Deletion of *srpABC*, *slvT*, and *slvAT* was verified by PCR and Sanger sequencing (Macrogen B.V., Amsterdam, The Netherlands).

Introduction of the complete *srp* operon (*srpRSABC*) and *slvAT* was accomplished using the mini-Tn7 delivery vector backbone of pBG35 developed by Zobel and colleagues (46). The DNA fragments were obtained by PCR using primer pairs listed on Table 4.2 and ligated into pBG35 plasmid at PacI and XbaI restriction site. This construct generated a Tn7 transposon segment in pBG35 containing gentamicin resistance marker and *srp* operon with Tn7 recognition sites flanking on 5' and 3' sides of the segment. Restriction analysis followed by DNA sequencing (Macrogen, The Netherlands) were performed to confirm the correct pBG-srp, pBG-slv, and pBG-srp-slv construct. The resulting construct was cloned in *E. coli* WM3064 and introduced into *P. putida* or *E. coli* strains with the help of *E. coli* WM3064 pTnS-1. Integration of construct into the Tn7 transposon segment was confirmed by gentamicin resistance, PCR, and the ability of the resulting transformants to withstand and grow under toluene atmosphere conditions.

Toxin-antitoxin assay

Bacterial growth during toxin-antitoxin assay was observed on LB medium supplemented with 100 mg liter^{-1} ampicillin and 50 mg liter^{-1} kanamycin. Starting cultures were inoculated from a 1:100 dilution of overnight culture (OD_{600} 0.1) into a microtiter plate (96 well), and bacterial growth was measured using a Tecan Spark 10M instrument. To induce toxin and antitoxin, a total concentration of 0.8% (wt/vol) arabinose and 2 mM IPTG were added to the culture, respectively. Cell morphology was observed using light microscope (Zeiss Axiolab 5) at a magnification of x100. A final concentration of 2.5x SYBR Green I (10000x stock; New England Biolabs) was applied to visualize DNA, followed by two times washing with 1x phosphate-buffer saline (PBS), and analyzed using a Guava easyCyte single sample flow cytometer (Millipore). At indicated time points, NAD^+ levels were measured using NAD/NADH-Glo assay kit (Promega) according to the manufacturer's manual. The percentage of NAD^+ level was calculated by dividing the measured luminescence of tested strains with that of the control strains at the same timepoints. RPPX_26255 and RPPX_26260 were modelled using I-TASSER server

(35) and visualized using PyMol (version 2.3.1). Phylogenetic trees of toxin-antitoxin module derived from COG5654-COG5642 family were constructed using MEGA (version 10.0.5) as a maximum likelihood tree with 100 bootstraps and visualized using iTOL webserver (https://itol.embl.de) (47).

Data availability

The sequence data for wild-type *P. putida* S12 and plasmid-cured genotypes of *P. putida* S12 ΔpTTS12 have been submitted to the SRA database under accession number PRJNA602416.

References

1. Aono R, Kobayashi H. 1997. Cell surface properties of organic solvent-tolerant mutants of *Escherichia coli* K-12. Appl Environ Microbiol 63:3637–3642.
2. Kabelitz N, Santos PM, Heipieper HJ. 2003. Effect of aliphatic alcohols on growth and degree of saturation of membrane lipids in *Acinetobacter calcoaceticus*. FEMS Microbiol Lett 220:223–227.
3. Hartmans S, van der Werf MJ, de Bont JA. 1990. Bacterial degradation of styrene involving a novel flavin adenine dinucleotide-dependent styrene monooxygenase. Appl Environ Microbiol 56:1347–1351.
4. Heipieper HJ, Weber FJ, Sikkema J, Keweloh H, de Bont JAM. 1994. Mechanisms of resistance of whole cells to toxic organic solvents. Trends Biotechnol 12:409–415.
5. Wierckx NJP, Ballerstedt H, de Bont JAM, Wery J. 2005. Engineering of solvent-tolerant *Pseudomonas putida* S12 for bioproduction of phenol from glucose. Appl Environ Microbiol 71:8221–8227.
6. Verhoef S, Wierckx N, Westerhof RGM, de Winde JH, Ruijssenaars HJ. 2009. Bioproduction of p-hydroxystyrene from glucose by the solvent-tolerant bacterium *Pseudomonas putida* S12 in a two-phase water-decanol fermentation. Appl Environ Microbiol 75:931–936.
7. Verhoef S, Ruijssenaars HJ, de Bont JAM, Wery J. 2007. Bioproduction of p-hydroxybenzoate from renewable feedstock by solvent-tolerant *Pseudomonas putida* S12. J Biotechnol 132:49–56.
8. Ruijssenaars HJ, Sperling EMGM, Wiegerinck PHG, Brands FTL, Wery J, de Bont JAM. 2007. Testosterone 15beta-hydroxylation by solvent tolerant *Pseudomonas putida* S12. J Biotechnol 131:205–208.
9. Koopman F, Wierckx N, de Winde JH, Ruijssenaars HJ. 2010. Efficient whole-cell biotransformation of 5-(hydroxymethyl)furfural into FDCA, 2,5-furandicarboxylic acid. Bioresour Technol 101:6291–6296.
10. Volkers RJM, de Jong AL, Hulst AG, van Baar BLM, de Bont JAM, Wery J. 2006. Chemostat-based proteomic analysis of toluene-affected *Pseudomonas putida* S12. Environ Microbiol 8:1674–1679.
11. Volkers RJM, Snoek LB, Ruijssenaars HJ, de Winde JH. 2015. Dynamic Response of *Pseudomonas putida* S12 to Sudden Addition of Toluene and the Potential Role of the

Solvent Tolerance Gene trgI. PLoS One 10:e0132416.

12. Kuepper J, Ruijssenaars HJ, Blank LM, de Winde JH, Wierckx N. 2015. Complete genome sequence of solvent-tolerant *Pseudomonas putida* S12 including megaplasmid pTTS12. J Biotechnol 200:17–18.
13. Kieboom J, Dennis JJ, de Bont JAM, Zylstra GJ. 1998. Identification and Molecular Characterization of an Efflux Pump Involved in *Pseudomonas putida* S12 Solvent Tolerance. J Biol Chem 273:85–91.
14. Kieboom J, Dennis JJ, Zylstra GJ, de Bont JA. 1998. Active efflux of organic solvents by *Pseudomonas putida* S12 is induced by solvents. J Bacteriol 180:6769–6772.
15. Garikipati SVBJ, McIver AM, Peeples TL. 2009. Whole-Cell Biocatalysis for 1-Naphthol Production in Liquid-Liquid Biphasic Systems. Appl Environ Microbiol 75:6545–6552.
16. Janardhan Garikipati SVB, Peeples TL. 2015. Solvent resistance pumps of *Pseudomonas putida* S12: Applications in 1-naphthol production and biocatalyst engineering. J Biotechnol 210:91–99.
17. O'Connor KE, Dobson ADW, Hartmans S. 1997. Indigo formation by microorganisms expressing styrene monooxygenase activity. Appl Environ Microbiol 63:4287–4291.
18. Isken S, de Bont JAM. 2000. The solvent efflux system of *Pseudomonas putida*. Appl Microbiol Biotechnol 54:711–714.
19. Shao Y, Harrison EM, Bi D, Tai C, He X, Ou HY, Rajakumar K, Deng Z. 2011. TADB: A web-based resource for Type 2 toxin-antitoxin loci in bacteria and archaea. Nucleic Acids Res.
20. Xie Y, Wei Y, Shen Y, Li X, Zhou H, Tai C, Deng Z, Ou HY. 2018. TADB 2.0: An updated database of bacterial type II toxin-antitoxin loci. Nucleic Acids Res 46:D749–D753.
21. Harms A, Brodersen DE, Mitarai N, Gerdes K. 2018. Toxins, Targets, and Triggers: An Overview of Toxin-Antitoxin Biology. Mol Cell 70:768–784.
22. Maisonneuve E, Gerdes K. 2014. Molecular mechanisms underlying bacterial persisters. Cell 157:539–548.
23. McKenzie JL, Robson J, Berney M, Smith TC, Ruthe A, Gardner PP, Arcus VL, Cook GM. 2012. A VapBC toxin-antitoxin module is a posttranscriptional regulator of metabolic flux in *Mycobacteria.* J Bacteriol 194:2189–2204.
24. Pinto UM, Pappas KM, Winans SC. 2012. The ABCs of plasmid replication and seg-

regation. Nat Rev Microbiol 10:755–765.

25. Trevors JT. 1986. Plasmid curing in bacteria. FEMS Microbiol Lett 32:149–157.
26. Chakrabarty AM. 1972. Genetic basis of the biodegradation of salicylate in *Pseudomonas*. J Bacteriol 112:815–823.
27. Wynands B, Lenzen C, Otto M, Koch F, Blank LM, Wierckx N. 2018. Metabolic engineering of *Pseudomonas taiwanensis* VLB120 with minimal genomic modifications for high-yield phenol production. Metab Eng 47:121–133.
28. Nikel PI, de Lorenzo V. 2018. *Pseudomonas putida* as a functional chassis for industrial biocatalysis: From native biochemistry to trans-metabolism. Metab Eng 50:142–155.
29. Studier FW, Moffatt BA. 1986. Use of bacteriophage T7 RNA polymerase to direct selective high-level expression of cloned genes. J Mol Biol 189:113–130.
30. Puigbò P, Bravo IG, Garcia-Vallve S. 2008. CAIcal: A combined set of tools to assess codon usage adaptation. Biol Direct 3:38.
31. Makarova KS, Wolf YI, Koonin E V. 2009. Comprehensive comparative-genomic analysis of Type 2 toxin-antitoxin systems and related mobile stress response systems in prokaryotes. Biol Direct 4:19.
32. Piscotta FJ, Jeffrey PD, Link AJ. 2019. ParST is a widespread toxin–antitoxin module that targets nucleotide metabolism. Proc Natl Acad Sci 116:826–834.
33. Skjerning RB, Senissar M, Winther KS, Gerdes K, Brodersen DE. 2018. The RES domain toxins of RES-Xre toxin-antitoxin modules induce cell stasis by degrading NAD. Mol Microbiol 66:213.
34. Freire DM, Gutierrez C, Garza-Garcia A, Grabowska AD, Sala AJ, Ariyachaokun K, Panikova T, Beckham KSH, Colom A, Pogenberg V, Cianci M, Tuukkanen A, Boudehen YM, Peixoto A, Botella L, Svergun DI, Schnappinger D, Schneider TR, Genevaux P, de Carvalho LPS, Wilmanns M, Parret AHA, Neyrolles O. 2019. An NAD^+ Phosphorylase Toxin Triggers *Mycobacterium tuberculosis* Cell Death. Mol Cell 73:1–10.
35. Yang J, Yan R, Roy A, Xu D, Poisson J, Zhang Y. 2015. The I-TASSER suite: Protein structure and function prediction. Nat Methods 12:7–8.
36. Murphy JR. 2011. Mechanism of diphtheria toxin catalytic domain delivery to the eukaryotic cell cytosol and the cellular factors that directly participate in the process. Toxins (Basel) 3:294–308.

37. Martínez-García E, de Lorenzo V. 2011. Engineering multiple genomic deletions in Gram-negative bacteria: analysis of the multi-resistant antibiotic profile of *Pseudomonas putida* KT2440. Environ Microbiol 13:2702–2716.

38. Holtwick R, Meinhardt F, Keweloh H. 1997. cis-trans isomerization of unsaturated fatty acids: Cloning and sequencing of the cti gene from *Pseudomonas putida* P8. Appl Environ Microbiol 63:4292–4297.

39. Pullinger GD, Lax AJ. 1992. A *Salmonella dublin* virulence plasmid locus that affects bacterial growth under nutrient-limited conditions. Mol Microbiol 6:1631–1643.

40. Zhang YX, Guo XK, Wu C, Bi B, Ren SX, Wu CF, Zhao GP. 2004. Characterization of a novel toxin-antitoxin module, VapBC, encoded by *Leptospira interrogans* chromosome. Cell Res 14:208–216.

41. Sun C, Guo Y, Tang K, Wen Z, Li B, Zeng Z, Wang X. 2017. MqsR/MqsA toxin/antitoxin system regulates persistence and biofilm formation in *Pseudomonas putida* KT2440. Front Microbiol 8:840.

42. Tamman H, Ainelo A, Ainsaar K, Hõrak R. 2014. A moderate toxin, GraT, modulates growth rate and stress tolerance of *Pseudomonas putida*. J Bacteriol 196:157–169.

43. Page R, Peti W. 2016. Toxin-antitoxin systems in bacterial growth arrest and persistence. Nat Chem Biol 12:208–214.

44. Muthuramalingam M, White JC, Bourne CR. 2016. Toxin-antitoxin modules are pliable switches activated by multiple protease pathways. Toxins 8:214.

45. Abril MA, Michan C, Timmis KN, Ramos JL. 1989. Regulator and enzyme specificities of the TOL plasmid-encoded upper pathway for degradation of aromatic hydrocarbons and expansion of the substrate range of the pathway. J Bacteriol 171:6782–6790.

46. Zobel S, Benedetti I, Eisenbach L, de Lorenzo V, Wierckx N, Blank LM. 2015. Tn7-Based Device for Calibrated Heterologous Gene Expression in *Pseudomonas putida*. ACS Synth Biol 4:1341–1351.

47. Letunic I, Bork P. 2019. Interactive Tree Of Life (iTOL) v4: recent updates and new developments. Nucleic Acids Res 47:W256–W25.

48. Bagdasarian M, Lurz R, Rückert B, Franklin FCH, Bagdasarian MM, Frey J, Timmis KN. 1981. Specific-purpose plasmid cloning vectors II. Broad host range, high copy number, RSF 1010-derived vectors, and a host-vector system for gene cloning in *Pseudomonas*. Gene 16:237–247.

49. Boyer HW, Roulland-dussoix D. 1969. A complementation analysis of the restriction and modification of DNA in *Escherichia coli*. J Mol Biol 41:459–472.

50. Herrero M, De Lorenzo V, Timmis KN. 1990. Transposon vectors containing non-antibiotic resistance selection markers for cloning and stable chromosomal insertion of foreign genes in gram-negative bacteria. J Bacteriol 172:6557–6567.

51. Figurski DH, Helinski DR. 1979. Replication of an origin-containing derivative of plasmid RK2 dependent on a plasmid function provided in trans. Proc Natl Acad Sci 76:1648–1652.

52. Choi K-H, Gaynor JB, White KG, Lopez C, Bosio CM, Karkhoff-Schweizer RR, Schweizer HP. 2005. A Tn7-based broad-range bacterial cloning and expression system. Nat Methods 2:443–448.

Supplementary Materials

Table 4.S1. Expression of *srpABC* genes in *P. putida* and *E. coli* strains in basal level and in the presence of 0.1% (vol/vol) toluene with *gyrB* and *rpoB* as reference genes

Genes	Strains	Basal expression	Toluene induced expression	Fold change
srpA	*P. putida* S12	1.69 ± 0.31	4.08 ± 0.79	2.44 ± 0.50
	P. putida S12-6.1	2.27 ± 0.36	4.56 ± 1.08	1.99 ± 0.28
	P. putida KT2440-srp	2.84 ± 0.92	5.60 ± 1.79	1.99 ± 0.28
	E. coli BL21(DE3)-srp	3.30 ± 0.43	6.60 ± 2.06	1.98 ± 0.45
	E. coli TG1-srp	5.28 ± 1.76	11.06 ± 4.10	2.10 ± 0.36
srpB	*P. putida* S12	1.92 ± 0.36	3.83 ± 0.76	2.02 ± 0.42
	P. putida S12-6.1	2.57 ± 0.33	5.49 ± 1.13	2.15 ± 0.46
	P. putida KT2440-srp	3.51 ± 1.22	6.59 ± 1.87	1.91 ± 0.20
	E. coli BL21(DE3)-srp	3.69 ± 0.58	7.52 ± 2.26	2.01 ± 0.36
	E. coli TG1-srp	5.35 ± 1.97	11.52 ± 4.84	2.21 ± 0.75
srpC	*P. putida* S12	2.01 ± 0.28	3.96 ± 0.75	1.97 ± 0.29
	P. putida S12-6.1	2.32 ± 0.27	4.45 ± 0.99	1.91 ± 0.35
	P. putida KT2440-srp	2.07 ± 0.68	5.13 ± 1.55	2.50 ± 0.22
	E. coli BL21(DE3)-srp	3.41 ± 0.52	6.70 ± 1.67	1.95 ± 0.25
	E. coli TG1-srp	4.18 ± 1.40	9.78 ± 5.23	2.32 ± 0.92

Table 4.S2. Codon adaptation index of *srp* operon in *E. coli* and *P. putida* reference strains

Genes	Length	CAI	%G+C	Nc	Species	Strain
srpA	1170	0.598	56.5	57.2	*E.coli*	K12
	1170	0.6	56.5	57.2	*E.coli*	B
	1170	0.742	56.5	57.2	*E.coli*	N/A
	1170	0.442	56.5	57.2	*P.putida*	F1
	1170	0.468	56.5	57.2	*P.putida*	N/A
	1170	0.372	56.5	57.2	*P.putida*	GB1
srpB	3150	0.662	56.5	46.1	*E.coli*	K12
	3150	0.67	56.5	46.1	*E.coli*	B
	3150	0.749	56.5	46.1	*E.coli*	N/A
	3150	0.565	56.5	46.1	*P.putida*	F1
	3150	0.587	56.5	46.1	*P.putida*	N/A
	3150	0.502	56.5	46.1	*P.putida*	GB1
srpC	1413	0.62	54.2	51.3	*E.coli*	K12
	1413	0.628	54.2	51.3	*E.coli*	B
	1413	0.735	54.2	51.3	*E.coli*	N/A
	1413	0.456	54.2	51.3	*P.putida*	F1
	1413	0.483	54.2	51.3	*P.putida*	N/A
	1413	0.394	54.2	51.3	*P.putida*	GB1
srpR	642	0.604	54.5	59.8	*E.coli*	K12
	642	0.622	54.5	59.8	*E.coli*	B
	642	0.724	54.5	59.8	*E.coli*	N/A
	642	0.464	54.5	59.8	*P.putida*	F1
	642	0.491	54.5	59.8	*P.putida*	N/A
	642	0.399	54.5	59.8	*P.putida*	GB1
srpS	780	0.636	55.4	55.5	*E.coli*	K12
	780	0.638	55.4	55.5	*E.coli*	B
	780	0.737	55.4	55.5	*E.coli*	N/A
	780	0.47	55.4	55.5	*P.putida*	F1
	780	0.496	55.4	55.5	*P.putida*	N/A
	780	0.399	55.4	55.5	*P.putida*	GB1

Table 4.S3. Putative COG5654-COG5642 RES-Xre toxin-antitoxin from NCBI RefSeq (31)

Strain	Protein ID	
	Toxin	Antitoxin
Acidovorax sp. JS42	YP_984893.1	YP_984894.1
Mycobacterium bovis BCG str. Pasteur 1173P2	YP_978095.1	YP_978096.1
Marinobacter hydrocarbonoclasticus VT8	YP_958617.1	YP_958618.1
Mycobacterium sp. KMS	YP_935598.1	YP_935597.1
Shewanella amazonensis SB2B	YP_928802.1	YP_928803.1
Shewanella sp. ANA-3	YP_863727.1	YP_863728.1
Gramella forsetii KT0803	YP_862703.1	YP_862704.1
Ralstonia eutropha H16	YP_840783.1	YP_840782.1
Burkholderia cenocepacia HI2424	YP_839838.1	YP_839837.1
Burkholderia cenocepacia HI2424	YP_837474.1	YP_837473.1
Rhodopseudomonas palustris BisA53	YP_780344.1	YP_780345.1
Rhodopseudomonas palustris BisA53	YP_778971.1	YP_778972.1
Burkholderia ambifaria AMMD	YP_777867.1	YP_777868.1
Burkholderia ambifaria AMMD	YP_777448.1	YP_777447.1
Burkholderia ambifaria AMMD	YP_777114.1	YP_777115.1
Rhizobium leguminosarum bv. viciae 3841	YP_771125.1	YP_771124.1
Rhizobium leguminosarum bv. viciae 3841	YP_771096.1	YP_771097.1
Rhizobium leguminosarum bv. viciae 3841	YP_765386.1	YP_765385.1
Rhizobium leguminosarum bv. viciae 3841	YP_764601.1	YP_764602.1
Nitrosomonas eutropha C91	YP_748179.1	YP_748180.1
Alkalilimnicola ehrlichii MLHE-1	YP_741338.1	YP_741337.1
Ralstonia eutropha H16	YP_725909.1	YP_725910.1
Trichodesmium erythraeum IMS101	YP_721262.1	YP_721261.1
Alcanivorax borkumensis SK2	YP_693226.1	YP_693225.1
Chelativorans sp. BNC1	YP_673203.1	YP_673204.1
Yersinia pestis Antiqua	YP_651606.1	YP_651605.1
Yersinia pestis Nepal516	YP_647735.1	YP_647734.1
Burkholderia cenocepacia AU 1054	YP_625684.1	YP_625683.1
Burkholderia cenocepacia AU 1054	YP_624375.1	YP_624376.1
Cupriavidus metallidurans CH34	YP_583373.1	YP_583374.1
Nitrobacter hamburgensis X14	YP_578969.1	YP_578968.1
Burkholderia xenovorans LB400	YP_552488.1	YP_552489.1
Polaromonas sp. JS666	YP_551796.1	YP_551795.1
Rhodopseudomonas palustris BisB18	YP_533769.1	YP_533770.1
Rhodopseudomonas palustris BisB18	YP_531278.1	YP_531277.1
Rhodoferax ferrireducens T118	YP_524055.1	YP_524056.1
Rhodopseudomonas palustris HaA2	YP_487787.1	YP_487786.1
Rhodopseudomonas palustris HaA2	YP_483989.1	YP_483990.1

Strain	Toxin	Antitoxin
Rhizobium etli CFN 42	YP_472228.1	YP_472227.1
Anaeromyxobacter dehalogenans 2CP-C	YP_464961.1	YP_464960.1
Erythrobacter litoralis HTCC2594	YP_457022.1	YP_457021.1
Salinibacter ruber DSM 13855	YP_446753.1	YP_446752.1
Salinibacter ruber DSM 13855	YP_444335.1	YP_444336.1
Rhodospirillum rubrum ATCC 11170	YP_428817.1	YP_428816.1
Rhodospirillum rubrum ATCC 11170	YP_428306.1	YP_428307.1
Rhodospirillum rubrum ATCC 11170	YP_427975.1	YP_427974.1
Rhodospirillum rubrum ATCC 11170	YP_425903.1	YP_425904.1
Brucella abortus 2308	YP_419077.1	YP_419076.1
Nitrosospira multiformis ATCC 25196	YP_411613.1	YP_411612.1
Synechococcus elongatus PCC 7942	YP_399513.1	YP_399514.1
Geobacter metallireducens GS-15	YP_384617.1	YP_384616.1
Burkholderia lata	YP_373007.1	YP_373008.1
Burkholderia lata	YP_366311.1	YP_366310.1
Rhodobacter sphaeroides 2.4.1	YP_353530.1	YP_353531.1
Pseudomonas fluorescens Pf0-1	YP_348851.1	YP_348852.1
Rhodobacter sphaeroides 2.4.1	YP_345300.1	YP_345299.1
Nitrosococcus oceani ATCC 19707	YP_342684.1	YP_342683.1
Thiobacillus denitrificans ATCC 25259	YP_315251.1	YP_315252.1
Ralstonia eutropha JMP134	YP_295535.1	YP_295536.1
Ralstonia eutropha JMP134	YP_293190.1	YP_293191.1
Pseudomonas syringae pv. phaseolicola 1448A	YP_273196.1	YP_273197.1
Pseudomonas protegens Pf-5	YP_257886.1	YP_257887.1
Pseudomonas syringae pv. syringae B728a	YP_233980.1	YP_233981.1
Brucella abortus bv. 1 str. 9-941	YP_223658.1	YP_223657.1
Aromatoleum aromaticum EbN1	YP_195457.1	YP_195458.1
Synechococcus elongatus PCC 6301	YP_171736.1	YP_171735.1
Aromatoleum aromaticum EbN1	YP_160869.1	YP_160870.1
Legionella pneumophila str. Paris	YP_123890.1	YP_123891.1
Burkholderia pseudomallei K96243	YP_111824.1	YP_111825.1
Legionella pneumophila subsp. pneumophila str. Philadelphia 1	YP_095631.1	YP_095632.1
Yersinia pseudotuberculosis IP 32953	YP_070779.1	YP_070778.1
Leifsonia xyli subsp. xyli str. CTCB07	YP_063014.1	YP_063013.1
Pectobacterium atrosepticum SCRI1043	YP_050894.1	YP_050895.1
Geobacter bemidjiensis Bem	YP_002136885.1	YP_002136886.1
Anaeromyxobacter sp. K	YP_002134448.1	YP_002134449.1
Cupriavidus taiwanensis LMG 19424	YP_002007827.1	YP_002007826.1
Cupriavidus taiwanensis LMG 19424	YP_002005344.1	YP_002005345.1
Chloroherpeton thalassium ATCC 35110	YP_001997574.1	YP_001997575.1

Strain	Toxin	Antitoxin
Rhodopseudomonas palustris TIE-1	YP_001992552.1	YP_001992551.1
Rhizobium etli CIAT 652	YP_001985675.1	YP_001985674.1
Burkholderia multivorans ATCC 17616	YP_001948023.1	YP_001948022.1
Burkholderia multivorans ATCC 17616	YP_001941953.1	YP_001941954.1
Brucella abortus S19	YP_001932799.1	YP_001932798.1
Methylobacterium populi BJ001	YP_001924424.1	YP_001924425.1
Burkholderia phytofirmans PsJN	YP_001890479.1	YP_001890478.1
Yersinia pseudotuberculosis PB1/+	YP_001872759.1	YP_001872758.1
Burkholderia phymatum STM815	YP_001863413.1	YP_001863414.1
Burkholderia phymatum STM815	YP_001863338.1	YP_001863339.1
Burkholderia phymatum STM815	YP_001860557.1	YP_001860558.1
Beijerinckia indica subsp. indica ATCC 9039	YP_001832632.1	YP_001832633.1
Burkholderia ambifaria MC40-6	YP_001815841.1	YP_001815840.1
Burkholderia ambifaria MC40-6	YP_001815740.1	YP_001815741.1
Burkholderia ambifaria MC40-6	YP_001812408.1	YP_001812407.1
Burkholderia ambifaria MC40-6	YP_001810424.1	YP_001810423.1
Burkholderia cenocepacia MC0-3	YP_001777325.1	YP_001777326.1
Burkholderia cenocepacia MC0-3	YP_001774298.1	YP_001774297.1
Shewanella woodyi ATCC 51908	YP_001761847.1	YP_001761846.1
Shewanella woodyi ATCC 51908	YP_001760834.1	YP_001760833.1
Yersinia pseudotuberculosis YPIII	YP_001720644.1	YP_001720645.1
Caulobacter sp. K31	YP_001686389.1	YP_001686390.1
Pseudomonas putida GB-1	YP_001668316.1	YP_001668315.1
Brucella suis ATCC 23445	YP_001622109.1	YP_001622110.1
Yersinia pestis Angola	YP_001606943.1	YP_001606942.1
Brucella canis ATCC 23365	YP_001594232.1	YP_001594233.1
Burkholderia multivorans ATCC 17616	YP_001585295.1	YP_001585294.1
Azorhizobium caulinodans ORS 571	YP_001527226.1	YP_001527227.1
Vibrio campbellii ATCC BAA-1116	YP_001447766.1	YP_001447765.1
Parvibaculum lavamentivorans DS-1	YP_001413635.1	YP_001413636.1
Xanthobacter autotrophicus Py2	YP_001409444.1	YP_001409443.1
Xanthobacter autotrophicus Py2	YP_001409339.1	YP_001409340.1
Yersinia pseudotuberculosis IP 31758	YP_001400767.1	YP_001400768.1
Ochrobactrum anthropi ATCC 49188	YP_001371470.1	YP_001371469.1
Sinorhizobium medicae WSM419	YP_001314122.1	YP_001314121.1
Sinorhizobium medicae WSM419	YP_001313272.1	YP_001313271.1
Sinorhizobium medicae WSM419	YP_001312332.1	YP_001312331.1
Mycobacterium tuberculosis F11	YP_001287957.1	YP_001287958.1
Mycobacterium tuberculosis H37Ra	YP_001283324.1	YP_001283325.1
Pseudomonas putida F1	YP_001268571.1	YP_001268572.1
Sphingomonas wittichii RW1	YP_001262457.1	YP_001262456.1

Strain	Toxin	Antitoxin
Sphingomonas wittichii RW1	YP_001260351.1	YP_001260352.1
Brucella ovis ATCC 25840	YP_001257308.1	YP_001257309.1
Legionella pneumophila str. Corby	YP_001250345.1	YP_001250346.1
Geobacter uraniireducens Rf4	YP_001231219.1	YP_001231220.1
Pseudomonas stutzeri A1501	YP_001172612.1	YP_001172613.1
Rhodobacter sphaeroides ATCC 17025	YP_001168572.1	YP_001168573.1
Novosphingobium aromaticivorans DSM 12444	YP_001166184.1	YP_001166185.1
Yersinia pestis Pestoides F	YP_001162176.1	YP_001162177.1
Polynucleobacter necessarius subsp. asymbioticus QLW-P1DM-WA-1	YP_001155131.1	YP_001155130.1
Mycobacterium gilvum PYR-GCK	YP_001136659.1	YP_001136660.1
Burkholderia vietnamiensis G4	YP_001115251.1	YP_001115250.1
Burkholderia vietnamiensis G4	YP_001114818.1	YP_001114817.1
Burkholderia vietnamiensis G4	YP_001114692.1	YP_001114691.1
Burkholderia vietnamiensis G4	YP_001110405.1	YP_001110406.1
Burkholderia vietnamiensis G4	YP_001109906.1	YP_001109907.1
Burkholderia pseudomallei 1106a	YP_001076500.1	YP_001076501.1
Mycobacterium sp. JLS	YP_001072829.1	YP_001072830.1
Mycobacterium sp. JLS	YP_001072800.1	YP_001072801.1
Burkholderia pseudomallei 668	YP_001063601.1	YP_001063602.1
Rhodobacter sphaeroides ATCC 17029	YP_001043985.1	YP_001043986.1
Methylibium petroleiphilum PM1	YP_001021529.1	YP_001021528.1
Yersinia enterocolitica subsp. enterocolitica 8081	YP_001006356.1	YP_001006355.1
Yersinia pestis biovar Microtus str. 91001	NP_993465.1	NP_993464.1
Rhodopseudomonas palustris CGA009	NP_948506.1	NP_948505.1
Ralstonia eutropha H16	NP_942832.1	NP_942831.1
Photorhabdus luminescens subsp. laumondii TTO1	NP_929604.1	NP_929603.1
Gloeobacter violaceus PCC 7421	NP_925671.1	NP_925670.1
Gloeobacter violaceus PCC 7421	NP_924158.1	NP_924159.1
Chromobacterium violaceum ATCC 12472	NP_899706.1	NP_899705.1
Bordetella bronchiseptica RB50	NP_889433.1	NP_889434.1
Bordetella parapertussis 12822	NP_885120.1	NP_885121.1
Bordetella pertussis Tohama I	NP_880058.1	NP_880057.1
Mycobacterium bovis AF2122/97	NP_855661.1	NP_855662.1
Nitrosomonas europaea ATCC 19718	NP_842117.1	NP_842116.1
Vibrio parahaemolyticus RIMD 2210633	NP_800280.1	NP_800279.1
Pseudomonas syringae pv. tomato str. DC3000	NP_790873.1	NP_790874.1
Pseudomonas putida KT2440	NP_744582.1	NP_744581.1
Brucella suis 1330	NP_699467.1	NP_699468.1
Yersinia pestis KIM10+	NP_669301.1	NP_669302.1
Brucella melitensis bv. 1 str. 16M	NP_541956.1	NP_541955.1

Strain	Toxin	Antitoxin
Sinorhizobium meliloti 1021	NP_437942.1	NP_437943.1
Sinorhizobium meliloti 1021	NP_437247.1	NP_437246.1
Sinorhizobium meliloti 1021	NP_436473.1	NP_436474.1
Sinorhizobium meliloti 1021	NP_436040.1	NP_436041.1
Yersinia pestis CO92	NP_405883.1	NP_405882.1
Agrobacterium fabrum str. C58	NP_353871.2	NP_353870.2
Mycobacterium tuberculosis CDC1551	NP_336505.1	NP_336506.1
Mycobacterium tuberculosis H37Rv	NP_216505.1	NP_216506.1
Mesorhizobium loti MAFF303099	NP_103613.1	NP_103614.1
Mesorhizobium loti MAFF303099	NP_085650.1	NP_085649.1
Sphingobium sp. YBL2	AJR25280.1	AJR25281.1
Pseudomonas putida S12	AJA16860.1	AJA16859.1

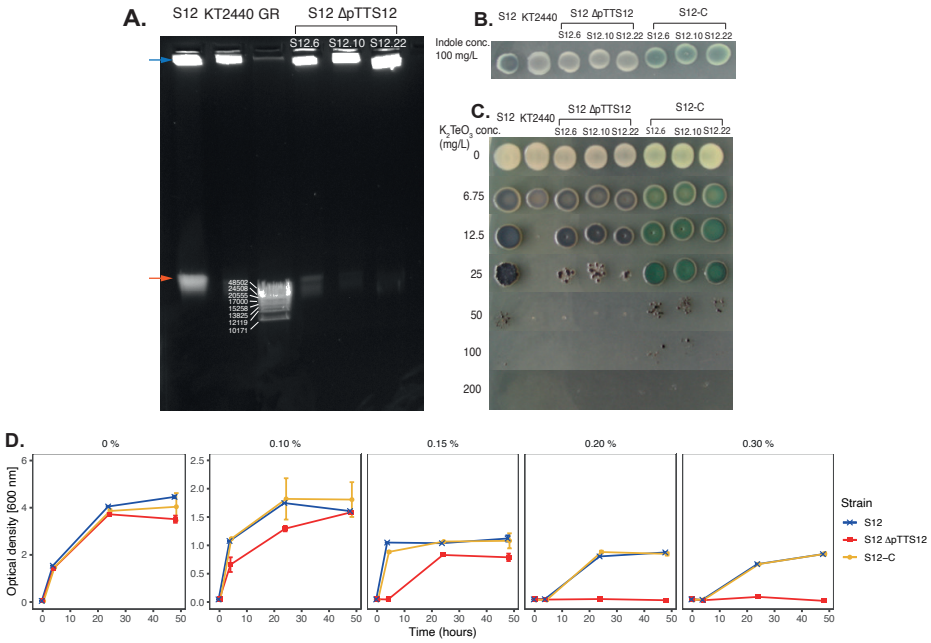

Fig. 4.S1. Removal and complementation of the megaplasmid pTTS12 from *P. putida* S12.

A. The loss of the megaplasmid band in megaplasmid-cured *P. putida* S12 proven by electrophoresis of agarose embedded genomic DNA. Megaplasmid band (orange arrow) was visible in the positive control *P. putida* S12 and absent in negative control *P. putida* KT2440 and Mitomycin C treated strains (strain S12-6, S12-10, and S12-22). Blue arrow indicates bacterial chromosome.

B. Activity of styrene monooxygenase (SMO) and styrene oxide isomerase (SOI) for indigo formation from indole in *P. putida* strains. Enzyme activity was lost in the megaplasmid-cured strains S12 ΔpTTS12 (white colonies) and restored with the complementation of megaplasmid in the strains S12-C (blue colonies). Indole (100 mg L^{-1}) was supplemented in M9 minimum media.

C. K_2TeO_3 resistance of *P. putida* strains on lysogeny broth (LB) agar. Tellurite resistance was reduced in the megaplasmid-cured strains S12 ΔpTTS12 (MIC 50 mg L^{-1}) and restored with the complementation of megaplasmid in the strains S12-C (MIC 200 mg L^{-1}).

D. Solvent tolerance analysis was performed on *P. putida* S12, *P. putida* S12 ΔpTTS12, and *P. putida* S12-C growing in liquid LB media with 0, 0.10, 0.15, 0.20 and 0.30 % v/v toluene. The removal of the megaplasmid pTTS12 clearly caused a significant reduction in the solvent tolerance of *P. putida* S12 ΔpTTS12. Complementation of pTTS12 restores the solvent tolerance trait in *P. putida* S12-C. This figure displays the mean of three independent replicates and error bars indicate standard deviation. The range of y-axis is different in the first panel (0 - 6) than the rest of the panels (0 - 2.5).

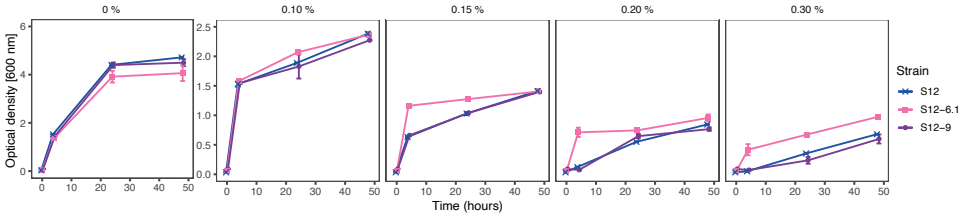

Fig. 4.S2. Metabolic burden of megaplasmid pTTS12 during growth in the presence of organic solvent.

Solvent tolerance was compared between *P. putida* S12, *P. putida* S12-6.1 (S12-6 srp::attn7), and *P. putida* S12-9 (S12-6 srp::attn7, pTTS12 tet::srp) in liquid LB media with 0, 0.10, 0.15, and 0.20 % v/v toluene. This figure displays the mean of three independent replicates and error bars indicate standard deviation. The range of y-axis is different in the first panel (0 - 6) than the rest of the panels (0 - 2.5).

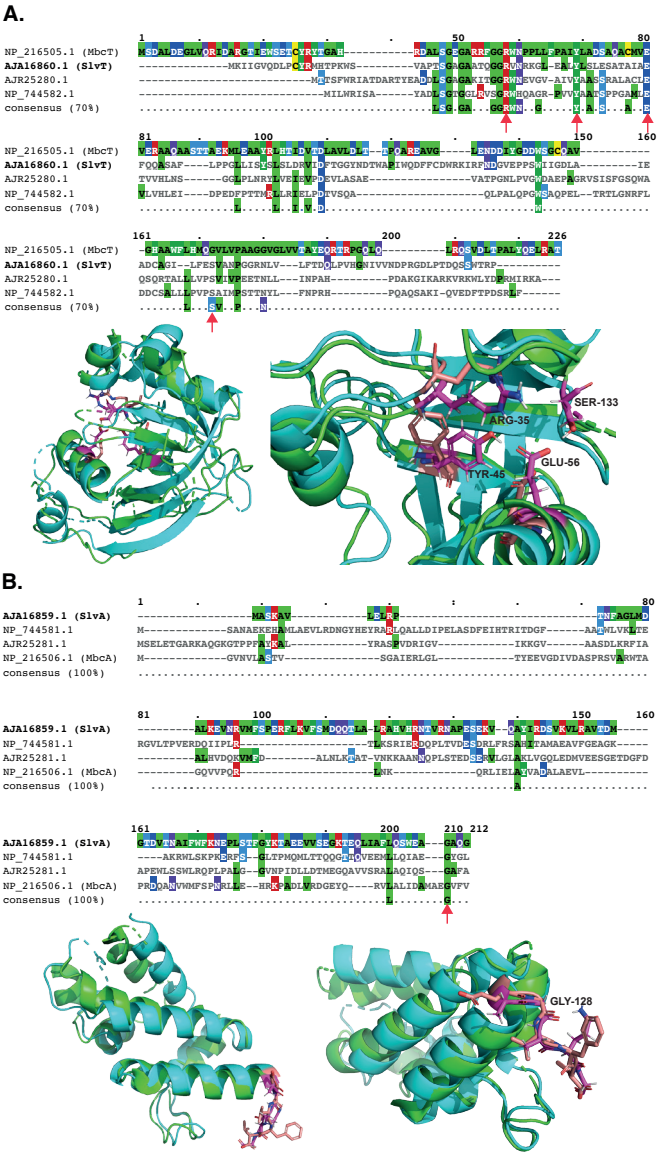

Fig. 4. S3. Multiple alignment of SlvT and SlvA with characterized toxin-antitoxin of COG5654- COG5642 family

A. Sequence similarity of SlvT from *P. putida* S12 with several characterized COG5654-family toxin protein and overlay of the predicted structure of SlvT (green) against the crystal structure of MbcT (turqoise). B. Sequence similarity of the SlvA from *P. putida* S12 with several characterized COG5642-family antitoxin protein and overlay of the predicted structure of SlvA (green) against the crystal structure of MbcA (turqoise). Putative active site residues which showed >70% similarities are indicated by arrows in the alignment or as magenta (SlvTA) and beige (MbcTA) sticks in the protein 3D structure overlay.